

Entanglement entropy of coherent intertwiner in loop quantum gravity

Gaoping Long ^{*1}, Qian Chen ^{†‡2}, and Jinsong Yang ^{§3}

¹College of Physics & Optoelectronic Engineering, Jinan University, Guangzhou, 510632, Guangdong, China

²Univ Lyon, Inria, ENS Lyon, UCBL, LIP, F-69342, Lyon Cedex 07, France

³School of Physics, Guizhou University, Guiyang 550025, China

Abstract

In this paper, we carry out the entanglement calculations on the coherent intertwiners. We first consider the entanglement introduced by the group-averaging of the tensor-product type intertwiner on a four-valents vertex. The result shows that the entanglement is determined by the probability distribution of recoupling spin, and this probability distribution is a well-behaved peak for the highest (and lowest) weight states. Further, we calculated explicitly the entanglement on gauge-invariant coherent intertwiner with four legs. Our numerical results show that the shape of the semiclassical polyhedron described by the coherent intertwiner can be related to the entanglement; In other words, the entanglement is controlled by the face-angle of the semiclassical polyhedron. Finally, we extend our analytical calculation to the coherent intertwiners with arbitrary number of legs.

1 Introduction

Though loop quantum gravity (LQG) provides a background-independent and non-perturbative quantum theory of General Relativity (GR) [1–6], the reconstruction of classical geometry in LQG is an unsettled crucial concern. Specifically, LQG defines the quantum states of spatial intrinsic and extrinsic geometry as spin-networks. The quantum geometry carried by spin-networks can be understood as the quantization of discrete twisted geometries [7–11], which is a generalization of the Regge geometry [12]. Then, the evolution of spin-networks is governed by the Hamiltonian operator in canonical formulation [13–16], or described by path-integral formulation [17–21]. This description of quantum gravity provides a discrete picture of quantum geometry at Plank scale, which indicates that the paradigm of classical smooth space-time geometry is just a semi-classical and large scale approximation. More explicitly, the information of quantum geometry encoded in spin-network states can be extracted by the geometric operators in LQG [22–26]; Correspondingly, the semi-classical geometries can be given by the expectation values of the geometric operators based on the coherent states, which are constructed by specific superposition of spin-networks [27–30]. However, the resulting semi-classical geometry takes the discrete formulation of twisted geometry, and they still need to be coarse-grained in order to derive the structure of smooth classical geometry [31]. This issue is a quite hard problem in LQG, so that a dynamical description of smooth geometry from the evolution of spin-networks is still an open question.

Nevertheless, there is another perspective which could provides us a guidance to recognize the coarse-grain. This idea is to study quantum statistical properties (e.g. the entanglement) on spin-networks, and establish the relation between them and the classical geometries (e.g. entropy-area law). In fact, the notion of quantum information is essential to a background independent quantum gravity: the relational perspective plays a very important role in the interpretation of the theory, which could be fully carried by the relations between local Hilbert spaces, namely, the structure of quantum entanglement. The studies following this idea have been carried out in many

*201731140005@mail.bnu.edu.cn

†chenqian.phys@gmail.com

‡corresponding author

§jsyang@gzu.edu.cn

works [32–39]. It has been shown that the (physical) entanglement carried by the spin-networks comes from the superpositions of spins and intertwiners. In fact, the physical states in LQG can be established by kinds of superpositions of spin-network basis. Thus, it is a question that which kind of superpositions of spin-network could give a realistic relation between the quantum statistics and the geometries. As mentioned above, by requiring the semi-classicality of the quantum geometry, the coherent states of spin-networks provides some superpositions of the spin-networks naturally [27–30, 40–43]. It is worth to explore the statistics based on such kind of superpositions of spin-networks, to relate them to the geometries at the semi-classical level. In fact, a gauge-variant coherent state of spin-network on a closed oriented graph is given by the product of the heat-kernel coherent state of $SU(2)$ on each edge. Such state carries no intertwiner entanglement [37]. Gauge averaging over the product state generates the coherent intertwiners at vertices, which introduce superposition and correlation onto the state thus the entanglement can access into the play. In this paper, we will focus on the mechanism of group averaging to the entanglement, specifically, of coherent intertwiners, which could be a preparation for the further related studies on the coherent state entanglement.

This paper is organized as follows. After the basic structure of spin-network state and intertwiner in LQG being introduced in section 2, the entanglements on kinds of spin-network state and intertwiners are calculated. Specifically, in section 3.1, we generalize the relation between boundary entanglement and intertwiner entanglement to the case that the internal edge carries spin-superposition; Then, we calculate the entanglement introduced by the group-averaging of the tensor-product type intertwiner with four legs by numerical method in section 3.2; Further, in section 3.3.1, this calculation is extended to the gauge-invariant coherent intertwiner with four legs; Moreover, in section 3.3.2, we also carry out some key analytical calculations for the entanglement on the coherent intertwiners with arbitrary number of legs. Finally, we finish with conclusion and outlook for further research in section 4 .

2 Spin-network state and intertwiner in loop quantum gravity

The Hilbert space \mathcal{H}_Γ for quantum geometry on a closed oriented graph Γ embedded in a 3-dimensional manifold is composed by the square integrable functions on $SU(2)$ associated to each edge $e \in \Gamma$, which are invariant under the $SU(2)$ action at every vertex $v \in \Gamma$. Specifically, a square integrable functions on Γ takes the formulation

$$\Psi_\Gamma = \Psi_\Gamma(\{h_e\}_{e \in \Gamma}). \quad (1)$$

The $SU(2)$ gauge invariance at the vertex of Ψ_Γ reads

$$\Psi_\Gamma(\{h_e\}_{e \in \Gamma}) = \Psi_\Gamma(\{g_{s(e)} h_e g_{t(e)}^{-1}\}_{e \in \Gamma}), \quad (2)$$

where g_v is given at each vertex $v \in \Gamma$ respectively, $s(e)$ represents the source vertex of e and $t(e)$ the target vertex of e . The spin-network states provide a basis of space \mathcal{H}_Γ . Specifically, a spin-network state on Γ is given by labeling a spin $j_e \in \frac{\mathbb{N}}{2}$ on each edge $e \in \Gamma$ and an intertwiner \mathcal{I}_v on each vertex $v \in \Gamma$, which reads [2]

$$\Psi_{\Gamma, \{j_e, \mathcal{I}_v\}} = \text{tr} \left(\bigotimes_{e \in \Gamma} \pi_{j_e}(h_e) \bigotimes_{v \in \Gamma} \mathcal{I}_v \right) \quad (3)$$

where $\pi_{j_e}(h_e)$ is the representation matrix of $h_e \in SU(2)$ in the representation space V^{j_e} of $SU(2)$ labelled by spin j_e , and $\mathcal{I}_v \in \bigotimes_{e|t(e)=v} V^{j_e} \otimes \bigotimes_{e|s(e)=v} \bar{V}^{j_e}$. Especially, the spin-network state $\Psi_{\Gamma, \{j_e, \mathcal{I}_v\}}$ is gauge invariant if and only if each $v \in \Gamma$ is labelled by a gauge invariant intertwiner. Another basis of space \mathcal{H}_Γ is given by the coherent state of spin-networks. The coherent state of spin-network is the superposition of spin-networks, which reads [27]

$$\Psi_{\Gamma, G}^t(h) = \prod_{e \in \Gamma} \Psi_{G_e}^t(h_e) \quad (4)$$

with

$$\Psi_{G_e}^t(h_e) := \sum_{j_e \in \frac{\mathbb{N}_+}{2}} (2j_e + 1) e^{-tj_e(j_e+1)/2} \chi_{j_e}(h_e G_e^{-1}), \quad (5)$$

where $G = \{G_e\}_{e \in \Gamma}$, $h = \{h_e\}_{e \in \Gamma}$, χ_j is the $SU(2)$ character with spin j and $t \propto \kappa \hbar$ is a semi-classicality parameter. As a function of the holonomies h_e , the coherent state is labelled by G_e , with $G_e \in T^*SU(2) \cong SL(2, \mathbb{C})$ being the complex coordinates of the discrete holonomy-flux phase space of LQG. The gauge invariant coherent state of spin-network is labelled by gauge equivalent class of $G_e \sim G_e^g := g_{s(e)}^{-1} G_e g_{t(e)}$ for all $e \in \Gamma$, where $g = \{g_v \in SU(2) | v \in \Gamma\}$. Equivalently, the gauge invariant coherent state of spin-network is also labelled by the gauge invariant intertwiners at each $v \in \Gamma$. Let us give an explicit introduction of gauge invariant intertwiner as follows.

The gauge invariant intertwiner \mathcal{I}_v at vertex v is a $SU(2)$ -invariant state in the tensor product space of all the spins associated to the edges linked to v ,

$$\mathcal{I}_v \in \mathcal{H}_v^{\{j_e\}} := \text{Inv}_{SU(2)} \left[\bigotimes_{e|t(e)=v} V^{j_e} \otimes \bigotimes_{e|s(e)=v} \bar{V}^{j_e} \right], \quad (6)$$

where \bar{V}^j is the dual space of V^j . The space V^j has dimension $d_j = (2j+1)$ and the orthonormal basis $\{|j, m\rangle | -j \leq m \leq j\}$, which diagonalize the $su(2)$ Casimir $\bar{J}^2 := J^i J_i, i = 1, 2, 3$ and the generator J_3 as

$$\bar{J}^2 |j, m\rangle = j(j+1) |j, m\rangle, \quad J_3 |j, m\rangle = m |j, m\rangle. \quad (7)$$

An orthonormal basis of the intertwiner space $\mathcal{H}_v^{\{j_e\}}$ is established by the recoupling scheme, which reads

$$\{\mathcal{I}_{v, \{j_i\}}^{\{j_e\}}\} = \mathcal{I}_{v, \{j_{i_1}, j_{i_2}, \dots, j_{i_{N_v-3}}\}}^{\{j_e\}} \in \mathcal{H}_v^{\{j_e\}}, \quad (8)$$

where N_v is the number of the edges which link to v , and $\{j_{i_1}, j_{i_2}, \dots, j_{i_{N_v-3}}\}$ labeling the internal edges in the recoupling scheme, which satisfies

$$\begin{aligned} |j_{e_1} - j_{e_2}| \leq j_{i_1} \leq j_{e_1} + j_{e_2}, \quad |j_{i_1} - j_{e_3}| \leq j_{i_2} \leq j_{i_1} + j_{e_3}, \\ \dots, |j_{i_{N_v-5}} - j_{e_{N_v-3}}| \leq j_{i_{N_v-4}} \leq j_{i_{N_v-5}} + j_{e_{N_v-3}}, \\ |j_{i_{N_v-4}} - j_{e_{N_v-2}}| \leq j_{i_{N_v-3}} \leq j_{i_{N_v-4}} + j_{e_{N_v-2}}, \\ |j_{e_{N_v-1}} - j_{e_{N_v}}| \leq j_{i_{N_v-3}} \leq j_{e_{N_v-1}} + j_{e_{N_v}}. \end{aligned} \quad (9)$$

Another basis of the intertwiner space $\mathcal{H}_v^{\{j_e\}}$ is the so-called coherent intertwiner basis [44, 45], which is established based on the $SU(2)$ coherent state. A $SU(2)$ coherent state $|j, \hat{n}\rangle$ is defined via rotating the highest weight state $|j, j\rangle$ by $g(\hat{n}) \in SU(2)$, namely [46],

$$|j, \hat{n}\rangle = g(\hat{n}) |j, j\rangle. \quad (10)$$

where \hat{n} is a unit vector, and $g(\hat{n}) \in SU(2)$ satisfies $\hat{n} = g(\hat{n}) \hat{z}$ with the north pole vector $\hat{z} = (0, 0, 1) \in \mathbb{S}^2$. The $SU(2)$ coherent state $|j, \hat{n}\rangle$ can be decomposed by the orthonormal basis $\{|j, m\rangle\}$ as [46]

$$|j, \hat{n}\rangle = \sum_{m=-j}^j c_{j,m}(\hat{n}) |j, m\rangle \quad (11)$$

with,

$$c_{j,m}(\hat{n}) = \left(\frac{(2j)!}{(j+m)!(j-m)!} \right)^{\frac{1}{2}} \left(-\sin \frac{\pi - \theta}{2} \right)^{j+m} \left(\cos \frac{\pi - \theta}{2} \right)^{j-m} \exp(-i(j+m)(\varphi + \pi)). \quad (12)$$

Moreover, the $SU(2)$ coherent states $|j, \hat{n}\rangle$ provide a overcomplete basis of the space V^j as

$$\mathbb{I}_{V^j} = (2j+1) \int_{\mathbb{S}^2} dn |j, \hat{n}\rangle \langle j, \hat{n}|, \quad (13)$$

where \mathbb{I}_{V^j} is the identity of V^j , and dn is the normalized measure on the 2-sphere \mathbb{S}^2 . Now, the coherent intertwiner basis of $\mathcal{H}_v^{\{j_e\}}$ can be given as

$$\mathbb{I}_{\mathcal{H}_v^{\{j_e\}}} = \int_{\mathbb{S}_v^{\{j_e\}}} d\sigma_v^{\{j_e\}} |\mathcal{I}_{v, \{j_e\}}^{\{\hat{n}_e\}}\rangle \langle \mathcal{I}_{v, \{j_e\}}^{\{\hat{n}_e\}}|, \quad (14)$$

where $\{\hat{n}_e\} \equiv (\hat{n}_{e_1}, \dots, \hat{n}_{e_{N_v}})$, $\mathcal{S}_v^{\{j_e\}} := \{(\hat{n}_{e_1}, \dots, \hat{n}_{e_{N_v}}) \in \times_{I=1}^{N_v} S_I^2 | \sum_{e|t(e)=v} j_e \hat{n}_e - \sum_{e|s(e)=v} j_e \hat{n}_e = 0\} / SU(2)$, $d\sigma_v^{\{j_e\}}$ is an invariant measure on $\mathcal{S}_v^{\{j_e\}}$, and the coherent intertwiner $|\mathcal{I}_{v,\{j_e\}}^{\{\hat{n}_e\}}\rangle$ is given by the following $SU(2)$ -group-averaging

$$|\mathcal{I}_{v,\{j_e\}}^{\{\hat{n}_e\}}\rangle := \int_{SU(2)} dg \bigotimes_{e|t(e)=v} g |j_e, \hat{n}_e\rangle \bigotimes_{e|s(e)=v} \langle j_e, \hat{n}_e | g^{-1}. \quad (15)$$

In order to simplify our notations and distinguish the labels of the in-going and out-going edges, we use j, \hat{n} to label the in-going edges and $\tilde{j}, \hat{\tilde{n}}$ to the out-going edges. Then, the coherent intertwiner can be reformulated as

$$|\mathcal{I}_{v,\{j,\tilde{j}\}}^{\{\hat{n},\hat{\tilde{n}}\}}\rangle := \int_{SU(2)} dg \bigotimes_{I=1}^P g |j_I, \hat{n}_I\rangle \bigotimes_{J=1}^Q \langle \tilde{j}_J, \hat{\tilde{n}}_J | g^{-1}, \quad (16)$$

where P is the number of the edges ended at v and Q is the number of the edges started at v .

The $SU(2)$ coherent states are said to be semi-classical states due to the property that they minimize the Heisenberg uncertainty relation [44, 46, 47]. A coherent spin state $|j, \hat{n}\rangle$ picks the unit vector \hat{n} by \vec{J} as $\hat{n} = \lim_{j \rightarrow \infty} \frac{\langle j, \hat{n} | \vec{J} | j, \hat{n} \rangle}{j}$. In the framework of LQG, each vertex $v \in \Gamma$ is dual to a polyhedron, and the edges attached to the v are dual to the faces of the polyhedron [48, 49]. The area and the normal vector of the face are characterized by j and \hat{n} from $|j, \hat{n}\rangle$ respectively. These pair-data $\{(j, \hat{n})\}$ indeed provides a semi-classical but gauge variant picture. The gauge invariance is fulfilled via $SU(2)$ -group-averaging over the tensoring spin states $\bigotimes_{e|t(e)=v} |j_e, \hat{n}_e\rangle \bigotimes_{e|s(e)=v} \langle j_e, \hat{n}_e |$ with $\{\hat{n}_e\} \in \mathcal{S}_v^{\{j_e\}}$, defining a gauge invariant coherent intertwiner. Although the information about the direction of each unit vector \hat{n}_e loses due to the $SU(2)$ -group-averaging, the relative angles amongst these unit vectors survive. Hence, a polyhedron in discrete geometry can be built from gauge invariant coherent intertwiners in a relational picture [44, 48, 49]: for a v around by N_v faces, the $\{j_e\}$ determines N_v areas and $\{\hat{n}_e\} \in \mathcal{S}_v^{\{j_e\}}$ determines $2N_v - 6$ relative angles.

3 Density matrix and entanglement entropy of coherent intertwiner

3.1 Boundary and intertwiner entanglement entropies

Consider a two-vertices graph Γ as illustrated in Fig.1: one vertex v_1 is attached by $P + 1$ edges and another vertex v_2 attached by $Q + 1$ edges, meanwhile v_1 and v_2 are connected by edge e . For the sake of simplifying the notations, we re-orient all of the edges to ensure that, e is out-going at v_1 and in-going at v_2 with other edges being in-going at v_1 and out-going at v_2 without losing generality. Then, the boundary Hilbert space for this system is defined as below

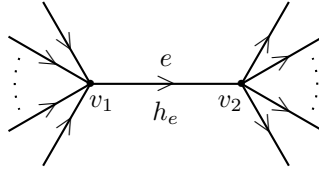


Figure 1: The two-vertex graph Γ . The holonomy h_e along the edge e that connects v_1 and v_2 contributes nothing to the entanglement entropy.

$$\mathcal{H}_{\partial\Gamma} := \bigotimes_{I=1}^P V^I \otimes \bigotimes_{J=1}^Q \bar{V}^J. \quad (17)$$

That is, excluding the Hilbert space associated with the internal edge e whose two-ends are contained in the graph. The apparent bipartition on the boundary Hilbert space is given by

$$\mathcal{H}_{\partial\Gamma} = \mathcal{H}_{v_1}^\partial \otimes \mathcal{H}_{v_2}^\partial, \quad \text{where } \mathcal{H}_{v_1}^\partial := \bigotimes_{I=1}^P V^I, \quad \text{and } \mathcal{H}_{v_2}^\partial := \bigotimes_{J=1}^Q \bar{V}^J. \quad (18)$$

On the other hand, the intertwiner Hilbert space on graph Γ is defined as below

$$\mathcal{H}_\Gamma := \mathcal{H}_{v_1} \otimes \mathcal{H}_{v_2}, \quad \text{where } \mathcal{H}_{v_1} := \text{Inv} \left(\bigotimes_{I=1}^P V_I \otimes \bar{V}_e \right) \text{ and } \mathcal{H}_{v_2} := \text{Inv} \left(V^e \otimes \bigotimes_{J=1}^Q \bar{V}_J \right). \quad (19)$$

The gluing map [37] provides a correspondence between the boundary state $|\psi_\Gamma\rangle_\partial \in \mathcal{H}_{\partial\Gamma}$ and the intertwiner state $|\psi_\Gamma\rangle \in \mathcal{H}_\Gamma$. Intuitively, the gluing map glues the boundary edges together along the internal edges. Let us illustrate the gluing map as follows. Assume that the internal edge e that links v_1 and v_2 carries a fixed j . Then, the spin-network state is written as

$$|\Psi_\Gamma^j\rangle = \sum_{\{j_I, \tilde{j}_J, j_i, \tilde{j}_i\}} \mathcal{C}_{\mathcal{I}_{v_1, \{j_i\}}^{\{j_I\}, j} \mathcal{I}_{v_2, \{\tilde{j}_i\}}^{\{\tilde{j}_J\}, j}} \underbrace{\left(\sum_{m, \{m_I\}} \mathcal{I}_{m_1 \dots m_P}^{j_1 \dots j_P j, \{j_i\}} \bigotimes_{I=1}^P |j_I, m_I\rangle \langle j, m| \right)}_{=|\mathcal{I}_{v_1, \{j_i\}}^{\{j_I\}, j}\rangle} \otimes \underbrace{\left(\sum_{n, \{\tilde{m}_J\}} |j, n\rangle \bigotimes_{J=1}^Q \langle \tilde{j}_J, \tilde{m}_J | \mathcal{I}_{n \tilde{m}_1 \dots \tilde{m}_Q}^{j \tilde{j}_1 \dots \tilde{j}_Q, \{\tilde{j}_i\}} \right)}_{=|\mathcal{I}_{v_2}^{\{\tilde{j}_J\}, j}\rangle}. \quad (20)$$

Let us explain the notations in this equation: (i) j_I, \tilde{j}_J label the boundary edges of Γ in left and right side respectively, and j_i, \tilde{j}_i represent the recoupling spins for the coherent intertwiner basis $\mathcal{I}_{v_1, \{j_i\}}^{\{j_I\}, j}$ and $\mathcal{I}_{v_2, \{\tilde{j}_i\}}^{\{\tilde{j}_J\}, j}$ respectively; (ii) The coefficients $\mathcal{I}_{m_1 \dots m_P}^{j_1 \dots j_P j, \{j_i\}}$ as well as $\mathcal{I}_{n \tilde{m}_1 \dots \tilde{m}_Q}^{j \tilde{j}_1 \dots \tilde{j}_Q, \{\tilde{j}_i\}}$ are responsible for the gauge invariances of $\mathcal{I}_{v_1, \{j_i\}}^{\{j_I\}, j}$ and $\mathcal{I}_{v_2, \{\tilde{j}_i\}}^{\{\tilde{j}_J\}, j}$ respectively, which can be constructed by concatenating Clebsch-Gordan coefficients; (iii) The coefficients $\mathcal{C}_{\mathcal{I}_{v_1, \{j_i\}}^{\{j_I\}, j} \mathcal{I}_{v_2, \{\tilde{j}_i\}}^{\{\tilde{j}_J\}, j}}$ encode the correlation between intertwiners living at v_1 and v_2 . On the other hand, the boundary state associated with the spin-network is written as

$$|\Psi_\Gamma^j\rangle_\partial = \sum_{\{j_I, \tilde{j}_J, j_i, \tilde{j}_i\}} \sqrt{2j+1} \mathcal{C}_{\mathcal{I}_{v_1, \{j_i\}}^{\{j_I\}, j} \mathcal{I}_{v_2, \{\tilde{j}_i\}}^{\{\tilde{j}_J\}, j}} \cdot \sum_{m, n, \{m_I, \tilde{m}_J\}} \mathcal{I}_{m_1 \dots m_P}^{j_1 \dots j_P j, \{j_i\}} \bigotimes_{I=1}^P |j_I, m_I\rangle D_{mn}^j(h_e) \bigotimes_{J=1}^Q \langle \tilde{j}_J, \tilde{m}_J | \mathcal{I}_{n \tilde{m}_1 \dots \tilde{m}_Q}^{j \tilde{j}_1 \dots \tilde{j}_Q, \{\tilde{j}_i\}}, \quad (21)$$

where $D_{mn}^j(h_e) := \langle j, m | h_e | j, n \rangle$. The gluing map is then viewed as sending $|\Psi_\Gamma^j\rangle$ to $|\Psi_\Gamma^j\rangle_\partial$, via sandwiching holonomy that associates the edge to-be-glued. This gluing map can be also established without the holonomy insertion (i.e., setting $h_e = \text{identity}$ in Eq. (21)), which leads to

$$|\check{\Psi}_\Gamma^j\rangle_\partial = \sum_{\{j_I, \tilde{j}_J, j_i, \tilde{j}_i\}} \sqrt{2j+1} \mathcal{C}_{\mathcal{I}_{v_1, \{j_i\}}^{\{j_I\}, j} \mathcal{I}_{v_2, \{\tilde{j}_i\}}^{\{\tilde{j}_J\}, j}} \sum_{m, \{m_I, \tilde{m}_J\}} \mathcal{I}_{m_1 \dots m_P}^{j_1 \dots j_P j, \{j_i\}} \bigotimes_{I=1}^P |j_I, m_I\rangle \bigotimes_{J=1}^Q \langle \tilde{j}_J, \tilde{m}_J | \mathcal{I}_{m \tilde{m}_1 \dots \tilde{m}_Q}^{j \tilde{j}_1 \dots \tilde{j}_Q, \{\tilde{j}_i\}}. \quad (22)$$

Now we look at the entanglement carried by these states. The intertwiner entanglement entropy $E(v_1|v_2)$ with respect to $\mathcal{H}_\Gamma = \mathcal{H}_{v_1} \otimes \mathcal{H}_{v_2}$ is given by the Von Neumann entropy from below reduced density matrix

$$\rho_{v_1}^j := \text{Tr}_{\mathcal{H}_{v_2}} |\Psi_\Gamma^j\rangle \langle \Psi_\Gamma^j| \quad (23)$$

$$= \sum_{\{j_I, j'_I, j_i, j'_i\}} \sum_{\{\tilde{j}_J, \tilde{j}'_J\}} \mathcal{C}_{\mathcal{I}_{v_1, \{j_i\}}^{\{j_I\}, j} \mathcal{I}_{v_2, \{\tilde{j}_i\}}^{\{\tilde{j}_J\}, j}} \overline{\mathcal{C}_{\mathcal{I}_{v_1, \{j'_i\}}^{\{j'_I\}, j} \mathcal{I}_{v_2, \{\tilde{j}'_i\}}^{\{\tilde{j}'_J\}, j}}} |\mathcal{I}_{v_1, \{j_i\}}^{\{j_I\}, j}\rangle \langle \mathcal{I}_{v_1, \{j'_i\}}^{\{j'_I\}, j}|. \quad (24)$$

On the other hand, the boundary entanglement entropy $E(v_1^\partial|v_2^\partial)$ with respect to $\mathcal{H}_{\partial\Gamma} = \mathcal{H}_{v_1}^\partial \otimes \mathcal{H}_{v_2}^\partial$ is given by the Von Neumann entropy from below reduced density matrix

$$\begin{aligned} \rho_{v_1}^{\partial, j} &:= \text{Tr}_{\mathcal{H}_{v_2}^\partial} |\Psi_\Gamma^j\rangle \langle \Psi_\Gamma^j|_\partial = \text{Tr}_{\mathcal{H}_{v_2}^\partial} |\check{\Psi}_\Gamma^j\rangle \langle \check{\Psi}_\Gamma^j|_\partial \quad (25) \\ &= \sum_{\{j_I, j'_I, j_i, j'_i\}} \sum_{\{\tilde{j}_J, \tilde{j}'_J\}} \mathcal{C}_{\mathcal{I}_{v_1, \{j_i\}}^{\{j_I\}, j} \mathcal{I}_{v_2, \{\tilde{j}_i\}}^{\{\tilde{j}_J\}, j}} \overline{\mathcal{C}_{\mathcal{I}_{v_1, \{j'_i\}}^{\{j'_I\}, j} \mathcal{I}_{v_2, \{\tilde{j}'_i\}}^{\{\tilde{j}'_J\}, j}}} \sum_{m, \{m_I, m'_I\}} \mathcal{I}_{m_1 \dots m_P}^{j_1 \dots j_P j, \{j_i\}} \overline{\mathcal{I}_{m'_1 \dots m'_P}^{j'_1 \dots j'_P j, \{j'_i\}}} \bigotimes_{I=1}^P |j_I, m_I\rangle \langle j'_I, m'_I| \end{aligned}$$

$$= \sum_{\{j_I, j'_I, \tilde{j}_I, \tilde{j}'_I\}} \sum_{\{\tilde{j}_J, \tilde{j}_I\}} \mathcal{C}_{\mathcal{I}_{v_1, \{j_i\}}^{\{j_I\}, j} \mathcal{I}_{v_2, \{\tilde{j}_i\}}^{\{\tilde{j}_J\}, j}} \overline{\mathcal{C}_{\mathcal{I}_{v_1, \{j'_i\}}^{\{j'_I\}, j} \mathcal{I}_{v_2, \{\tilde{j}'_i\}}^{\{\tilde{j}'_J\}, j}}} \sum_m \langle j, m | \mathcal{I}_{v_1, \{j_i\}}^{\{j_I\}, j} \rangle \langle \mathcal{I}_{v_1, \{j'_i\}}^{\{j'_I\}, j} | j, m \rangle, \quad (26)$$

where $\mathcal{H}_{v_2}^\partial = \bigotimes_{j=1}^Q \bar{V}_j$ is the boundary-edge state space attached to the vertex v_2 , and below orthogonality is used

$$\sum_{\{m_I\}_{I=1}^N} \mathcal{I}_{m_1 \dots m_N}^{j_1 \dots j_N j, \{j_i\}} \overline{\mathcal{I}_{m_1 \dots m_N}^{j_1 \dots j_N j', \{j'_i\}}} = \frac{1}{2j+1} \delta_{jj'} \delta_{mm'} \delta_{\{j_i\} \{j'_i\}}. \quad (27)$$

Indeed, one can verify the normalization $\text{Tr}_{\mathcal{H}_{v_1}^\partial} \rho_{v_1}^{\partial, j} = 1$. Note that the relation between the two density matrices can be given by

$$\rho_{v_1}^{\partial, j} = \text{Tr}_{V_e} \rho_{v_1}^j \quad (28)$$

with $V_e = V^j$. That is to say, the reduced density matrix $\rho_{v_1}^{\partial, j}$ of the half-cut boundary can be understood as tracing the reduced density matrix $\rho_{v_1}^j$ of the half-cut graph over the recoupled Hilbert space (here, it is V^j associative with the spin- j along the internal edge e). Then, following [37] one can show a simple relation between the entanglement entropy of $\mathcal{H}_{\partial\Gamma} = \mathcal{H}_{v_1}^\partial \otimes \mathcal{H}_{v_2}^\partial$ and of $\mathcal{H}_\Gamma = \mathcal{H}_{v_1} \otimes \mathcal{H}_{v_2}$.

Theorem 1. *In the cases that the spin along the internal edge is fixed at j , the following relation between entanglement entropies holds*

$$E_j(v_1^\partial | v_2^\partial) = E_j(v_1 | v_2) + \ln(2j+1), \quad (29)$$

where $E_j(v_1^\partial | v_2^\partial) := -\text{Tr}(\rho_{v_1}^{\partial, j} \ln \rho_{v_1}^{\partial, j})$ and $E_j(v_1 | v_2) := -\text{Tr}(\rho_{v_1}^j \ln \rho_{v_1}^j)$.

The relation Eq.(29) between boundary entanglement and intertwiner entanglement can be generalized straightforwardly to the cases that the internal edge e carries spin-superposition. More explicitly, one can consider the state

$$|\Psi_\Gamma\rangle = \sum_j \alpha_j |\Psi_\Gamma^j\rangle = \sum_j \sum_{\{j_I, \tilde{j}_J, \tilde{j}_I, \tilde{j}_I\}} \alpha_j \mathcal{C}_{\mathcal{I}_{v_1, \{j_i\}}^{\{j_I\}, j} \mathcal{I}_{v_2, \{\tilde{j}_i\}}^{\{\tilde{j}_J\}, j}} |\mathcal{I}_{v_1, \{j_i\}}^{\{j_I\}, j}\rangle \otimes |\mathcal{I}_{v_2, \{\tilde{j}_i\}}^{\{\tilde{j}_J\}, j}\rangle, \quad (30)$$

the gluing state with holonomy insertion

$$\begin{aligned} |\Psi_\Gamma\rangle_\partial &= \sum_j \alpha_j \sum_{\{j_I, \tilde{j}_J, \tilde{j}_I, \tilde{j}_I\}} \sqrt{2j+1} \mathcal{C}_{\mathcal{I}_{v_1, \{j_i\}}^{\{j_I\}, j} \mathcal{I}_{v_2, \{\tilde{j}_i\}}^{\{\tilde{j}_J\}, j}} \\ &\cdot \sum_{m, n, \{m_I, \tilde{m}_J\}} \mathcal{I}_{m_1 \dots m_P}^{j_1 \dots j_P j, \{j_i\}} \bigotimes_{I=1}^P |j_I, m_I\rangle D_{mn}^j(h_e) \bigotimes_{J=1}^Q |\tilde{j}_J, \tilde{m}_J\rangle \mathcal{I}_{\tilde{m}_1 \dots \tilde{m}_Q}^{\tilde{j}_1 \dots \tilde{j}_Q, \{\tilde{j}_i\}}, \end{aligned} \quad (31)$$

and the gluing state without holonomy insertion

$$\begin{aligned} &|\check{\Psi}_\Gamma\rangle_\partial \\ &= \sum_j \alpha_j \sum_{\{j_I, \tilde{j}_J, \tilde{j}_I, \tilde{j}_I\}} \sqrt{2j+1} \mathcal{C}_{\mathcal{I}_{v_1, \{j_i\}}^{\{j_I\}, j} \mathcal{I}_{v_2, \{\tilde{j}_i\}}^{\{\tilde{j}_J\}, j}} \sum_{m, \{m_I, \tilde{m}_J\}} \mathcal{I}_{m_1 \dots m_P}^{j_1 \dots j_P j, \{j_i\}} \bigotimes_{I=1}^P |j_I, m_I\rangle \bigotimes_{J=1}^Q |\tilde{j}_J, \tilde{m}_J\rangle \mathcal{I}_{\tilde{m}_1 \dots \tilde{m}_Q}^{\tilde{j}_1 \dots \tilde{j}_Q, \{\tilde{j}_i\}}. \end{aligned} \quad (32)$$

Again, the reduced density matrices are obtained via partial tracing in $\mathcal{H}_{v_2}^\partial$ and \mathcal{H}_{v_2} respectively, which gives,

$$\tilde{\rho}_{v_1}^\partial := \text{Tr}_{\mathcal{H}_{v_2}^\partial} |\Psi_\Gamma\rangle \langle \Psi_\Gamma|_\partial = \text{Tr}_{\mathcal{H}_{v_2}^\partial} |\check{\Psi}_\Gamma\rangle \langle \check{\Psi}_\Gamma|_\partial, \quad (33)$$

and

$$\tilde{\rho}_{v_1} := \text{Tr}_{\mathcal{H}_{v_2}} |\Psi_\Gamma\rangle \langle \Psi_\Gamma|. \quad (34)$$

Similarly, the generalized relation between $\tilde{\rho}_{v_1}^\partial$ and $\tilde{\rho}_{v_1}$ holds by taking superposition of j into account, which reads

$$\tilde{\rho}_{v_1}^\partial = \text{Tr}_{V_e} \tilde{\rho}_{v_1}, \quad (35)$$

where $V_e = \bigoplus_j V^j$ and $\tilde{\rho}_{v_1} = \bigoplus_j \tilde{\rho}_j \rho_{v_1}^j$ with $\tilde{\rho}_j \equiv \alpha_j \bar{\alpha}_j$. Then, the relation between intertwiners and boundary entanglements leads the following Theorem.

Theorem 2. *In the cases that the spin along the internal edge is superposed, say the intertwiner state is given by $|\Psi_\Gamma\rangle$, then the following relation between entanglement entropies holds*

$$E(v_1^\partial|v_2^\partial) = \sum_j \tilde{p}_j \ln(2j+1) - \sum_j \tilde{p}_j \ln \tilde{p}_j + \sum_j \tilde{p}_j E_j(v_1|v_2), \quad (36)$$

where $E(v_1^\partial|v_2^\partial) := -\text{Tr}(\tilde{\rho}_{v_1}^\partial \ln \tilde{\rho}_{v_1}^\partial)$ and $E_j(v_1|v_2) = -\text{Tr}(\rho_{v_1}^j \ln \rho_{v_1}^j)$.

Let us have a discussion on the above Theorem. First, referring to [37], the first term in Eq.(36) should be interpreted as coming from gauge-breaking, and it follows that the second and the third terms should be interpreted as the intertwiner entanglement, since the $-\sum_j \tilde{p}_j \ln \tilde{p}_j$ comes from the spin-superposition along the linking edge e , and the $E_j(v_1|v_2)$ is the intertwiner entanglement when the spin is fixed. Second, in the case of single internal edge graph, it has been shown that the holonomy along the internal edge e plays no role in the entanglement entropy in Ref. [37] for fixed j , and Eq.(33) in our calculation extends this point to the case of superposed j ; Indeed, one is able to gauge-fix the h_e into identity, and then $|\Psi_\Gamma\rangle_\partial$ becomes $|\check{\Psi}_\Gamma\rangle_\partial$ which can be regarded as an intertwiner on a single vertex as illustrated in Fig. 2; Notice that Eq.(33) tells us that $|\Psi_\Gamma\rangle_\partial$ and $|\check{\Psi}_\Gamma\rangle_\partial$ have the same reduced density matrix, thus the respect entanglement entropies depicted in Fig. 2 are indistinguishable. Third, while above general formalism is still vague for the sake of establishing relation between the entanglement and geometry, the coherent intertwiners provide a semi-classical picture of geometry on polyhedron, which could interlace the genuine quantum notion — entanglement, with the discrete geometry. In the following part of this paper, we are going to explore how the entanglement entropy emerges from this semi-classical picture, and how the entanglement gets reflected in the discrete geometry, or in turn.

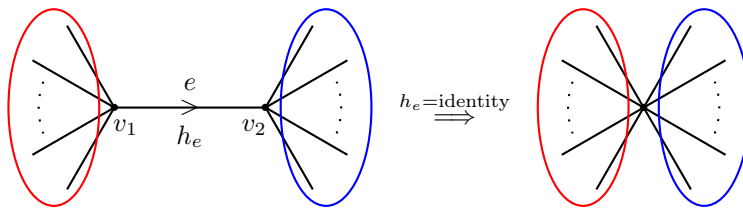


Figure 2: The left graph (two-vertex) has the same entanglement entropy between boundary edges with the right graph (one-vertex).

3.2 Entanglement produced from group-averaging

As a prelude for the study on coherent intertwiner, this part is meant to show how entanglement can be produced from group averaging. We begin with a gauge variant scenario based on the graph with only one vertex v , and the corresponding wave-function is below tensor state,

$$\bigotimes_{e|t(e)=v} |j_e, m_e\rangle \otimes \bigotimes_{e|s(e)=v} \langle j_{e'}, m_{e'}| \in \bigotimes_{e|t(e)=v} V^{j_e} \otimes \bigotimes_{e|s(e)=v} \bar{V}^{j_{e'}}. \quad (37)$$

This is not a physical spin-network due to the absence of gauge invariance, and there is also no entanglement. To get a gauge invariant state, the group-averaging is adopted, which inevitably introduces superposition and entanglement. It is possible to grant the physical implication for the group-averaging by considering some $SU(2)$ invariant measurement: suppose that we are given a set $\{|\phi_i\rangle\}_i$ whose members are all $SU(2)$ -invariant pointer-states $|\phi_i\rangle$, i.e., $|\phi_i\rangle = g|\phi_i\rangle$ for any $g \in SU(2)$, then this invariance can be conveyed to the probability distribution $|\langle \phi_i|\psi\rangle|^2$ where $|\psi\rangle$ is the state to be observed, because

$$\langle \phi_i|\psi\rangle = \int_{SU(2)} dg \langle g\phi_i|\psi\rangle = \int_{SU(2)} dg \langle \phi_i|g^\dagger\psi\rangle = \langle \phi_i|\int_{SU(2)} dg |g^\dagger\psi\rangle. \quad (38)$$

It is clear that $\int_{SU(2)} dg |g^\dagger\psi\rangle$ is $SU(2)$ -invariant. This group-averaging process can be viewed as a particular ‘twirling’, say $\rho \mapsto \int_{SU(2)} dg (g\rho g^\dagger)$ in the field of quantum information, with slightly different that the group-average here is based on a pure state $|\psi\rangle$ and getting another pure state $\int_{SU(2)} dg |g^\dagger\psi\rangle$, while twirling can be implemented on any state, and usually getting a mixed state.

The rest of this part will calculate the entanglement introduced by the group-averaging. Let us look at an example. Consider the graph with only one four-valents' vertex v and the intertwiner space $\check{\mathcal{H}}_v^{\{j_1, j_2, j_3, j_4\}} = V^{j_1} \otimes V^{j_2} \otimes \bar{V}^{j_3} \otimes \bar{V}^{j_4}$ on v . An element in $\check{\mathcal{H}}_v^{\{j_1, j_2, j_3, j_4\}}$ is given by the tensor product as below,

$$|j_1, m_1\rangle \otimes |j_2, m_2\rangle \otimes \langle j_3, m_3| \otimes \langle j_4, m_4|, \quad (39)$$

where we take the four-valents' bipartition $(2, 2)$, with the two left-side edges being ingoing and the two right-side edges being outgoing. Clearly, there is no entanglement between left and right sides, say $E(A|B) = 0$ with $\mathcal{H}_A := V^{j_1} \otimes V^{j_2}$ and $\mathcal{H}_B := \bar{V}^{j_3} \otimes \bar{V}^{j_4}$. Now, let us implement the $SU(2)$ -group-averaging over the tensor state, which leads

$$\begin{aligned} |\check{\mathcal{I}}\rangle &= \int_{SU(2)} dg g|j_1, m_1\rangle \otimes g|j_2, m_2\rangle \otimes \langle j_3, m_3|g^{-1} \otimes \langle j_4, m_4|g^{-1} \\ &= \sum_j \sum_{k, m=-j}^j \sum_{\vec{k}} \frac{1}{2j+1} C_{k_1 k_2 k}^{j_1 j_2 j} \overline{C_{m_1 m_2 m}^{j_1 j_2 j}} C_{k_3 k_4 k}^{j_3 j_4 j} C_{m_3 m_4 m}^{j_3 j_4 j} |j_1, k_1\rangle \otimes |j_2, k_2\rangle \otimes \langle j_3, k_3| \otimes \langle j_4, k_4|, \end{aligned} \quad (40)$$

where $\vec{k} \equiv \{k_1, k_2, k_3, k_4\}$, $C_{m_1 m_2 m}^{j_1 j_2 j} \equiv \langle j_1, m_1, j_2, m_2 | j, m \rangle$ stands for Clebsch-Gordan coefficient. One should note that the group-averaging spoils the normalization so it should be retrieved by rescaling later. In addition, recall that $\vec{m} \equiv \{m_1, m_2, m_3, m_4\}$ are fixed, the $SU(2)$ -group-averaging will eliminate some configuration that do not satisfy $m_1 + m_2 = m_3 + m_4$. This is the closure condition on magnetic quantum numbers. The state $|\check{\mathcal{I}}\rangle$ survived from the group-averaging is a gauge invariant state, and it can be also viewed as a bipartite system between two sets of recoupled spins, see the illustration in Fig.3. To simplify the expression, let us rewrite $|\check{\mathcal{I}}\rangle$ as

$$|\check{\mathcal{I}}\rangle = \sum_{j, k} \frac{1}{2j+1} f(j, \vec{j}, \vec{m}) |j_1, j_2; j, k\rangle \otimes \langle j_3, j_4; j, k|, \quad (41)$$

where $|j_1, j_2; j, k\rangle := \sum_{\{k_1, k_2\}} C_{k_1 k_2 k}^{j_1 j_2 j} |j_1, k_1\rangle \otimes |j_2, k_2\rangle$ defines a recoupled spin, likewise for $\langle j_3, j_4; j, k|$, and we denote

$$f(j, \vec{j}, \vec{m}) \equiv \sum_m \overline{C_{m_1 m_2 m}^{j_1 j_2 j}} C_{m_3 m_4 m}^{j_3 j_4 j} \quad (42)$$

for the fixed $\vec{j} \equiv \{j_1, j_2, j_3, j_4\}$ and \vec{m} .

Recall the bipartition $\mathcal{H}_A := V^{j_1} \otimes V^{j_2}$ and $\mathcal{H}_B := \bar{V}^{j_3} \otimes \bar{V}^{j_4}$. Then, the entanglement $E(A|B)$ between A and B can be given by the Von Neumann entropy of the reduced density matrices ρ_A . For the state $|\check{\mathcal{I}}\rangle$, the reduced density matrix ρ_A is defined by $\rho_A := \text{Tr}_B(\rho_{\check{\mathcal{I}}})$ with $\rho_{\check{\mathcal{I}}} \equiv \frac{|\check{\mathcal{I}}\rangle\langle\check{\mathcal{I}}|}{\langle\check{\mathcal{I}}|\check{\mathcal{I}}\rangle}$. More explicitly, one has

$$\rho_A = \frac{1}{\langle\check{\mathcal{I}}|\check{\mathcal{I}}\rangle} \sum_j \sum_{k=-j}^j \frac{|f(j, \vec{j}, \vec{m})|^2}{(2j+1)^2} |j_1, j_2; j, k\rangle \langle j_1, j_2; j, k|. \quad (43)$$

One can introduce the probability distribution p_j of the recoupling spin j , which is given by $p_j = \frac{|f(j, \vec{j}, \vec{m})|^2}{(2j+1)\langle\check{\mathcal{I}}|\check{\mathcal{I}}\rangle}$, and the reduced density matrix can be decomposed into ρ_j^A , i.e.,

$$\rho_A = \sum_j p_j \rho_j^A, \quad \rho_j^A = \sum_{k=-j}^j \frac{|j_1, j_2; j, k\rangle \langle j_1, j_2; j, k|}{(2j+1)}. \quad (44)$$

It is clear that the \mathcal{H}_A and \mathcal{H}_B are entangled for the state $|\check{\mathcal{I}}\rangle$. The entanglement entropy $E(A|B) := -\text{Tr}(\rho_A \ln \rho_A)$ is determined by the distribution p_j , which reads

$$E(A|B) = E_p(A|B) + E_0(A|B), \quad E_p(A|B) := -\sum_j (p_j \ln p_j), \quad E_0(A|B) := \sum_j p_j S_j^A, \quad (45)$$

where $S_j^A := -\text{Tr}(\rho_j^A \ln \rho_j^A) = \ln(2j+1)$. Further, the distribution p_j and the entanglement entropy $E(A|B)$ can be calculated numerically. The numerical results of p_j are illustrated in Figs.4,5 and 6,

which show that the distribution p_j is oscillating with respect to j for small $\{m_1, m_2, m_3, m_4\}$ state, while there is a peak for highest (and lowest) weight state. The numerical values of entanglement entropy $E(A|B)$ are listed in Tabs. 1 and 2, which show that the entanglement entropy can be controlled by the magnetic configurations.

It is worth to have a discussion on these results. First, one should notice that the quantum number $\{m_1, m_2, m_3, m_4\}$ are gauge variant, and their geometric interpretation become fuzzy after group-averaging. Second, note that the distribution p_j is a peak for highest (and lowest) weight state, it ensures that the entanglement entropy is able to capture the main character of the distribution p_j . By combining these two points, it is reasonable to consider the entanglement carried by gauge invariant coherent intertwiners, since they are constructed by the highest (and lowest) weight state and they describe semiclassical geometry on polyhedrons. In next subsection, we will focus on the coherent intertwiners which provide a semiclassical picture of polyhedron geometry, and one may expect that both entanglement, superposition, and the geometric picture could be drawn by the gauge invariant knowledge encoded in the area-weighted normal vectors $\{j_e \hat{n}_e\}$ labelling the coherent intertwiners.

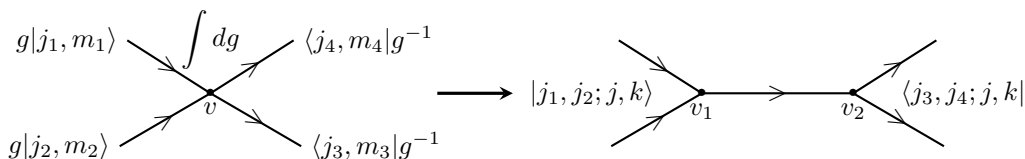


Figure 3: The $SU(2)$ -group-averaging produces entanglement between the legs. This can be viewed as the entanglement between two coupled states $|j_1, j_2; j, k\rangle$ and $\langle j_3, j_4; j, k|$ at v_1 and v_2 , respectively.

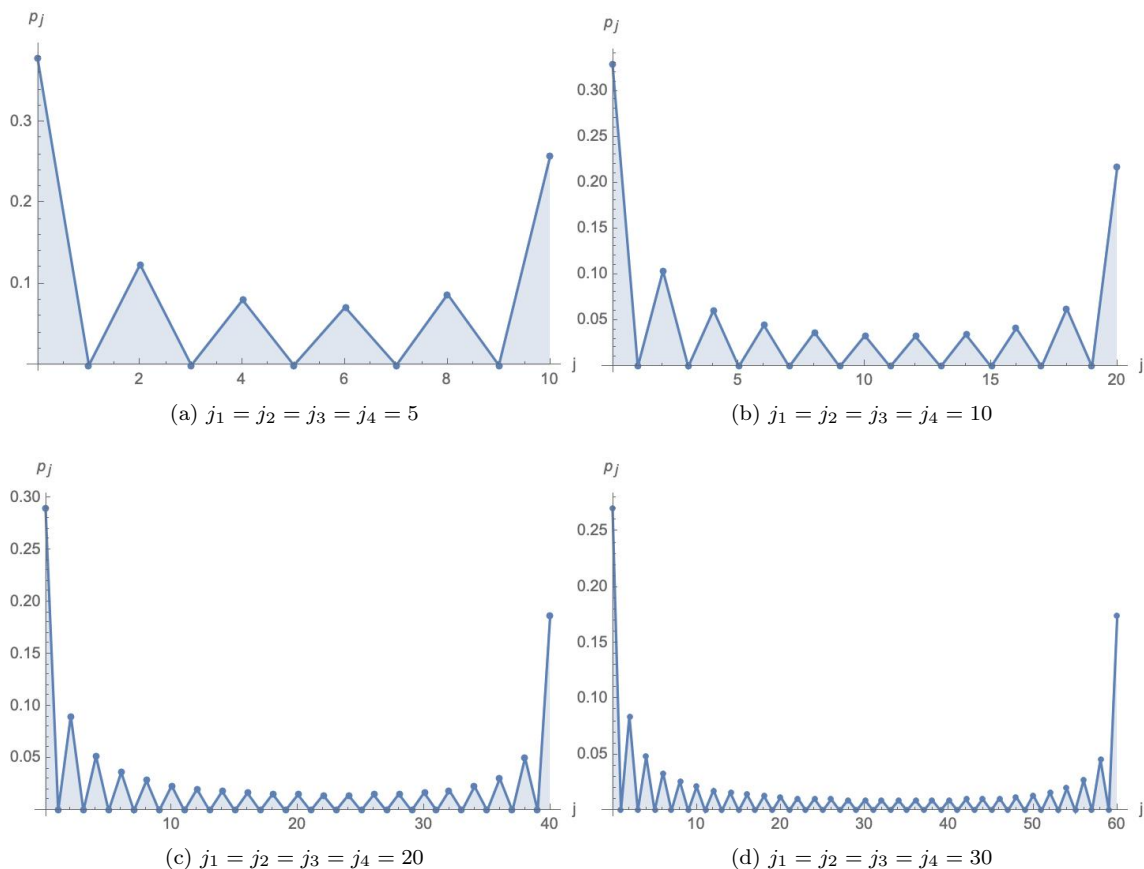


Figure 4: The numerical results of p_j for $(m_1, m_2, m_3, m_4) = (0, 0, 0, 0)$ and $j_1 = j_2 = j_3 = j_4 = 5, 10, 20, 30$, where the x -axis shows the recouping spin j and y -axis shows the numerical value of p_j . These figures show that p_j has an oscillation with respect to coupling spin j .

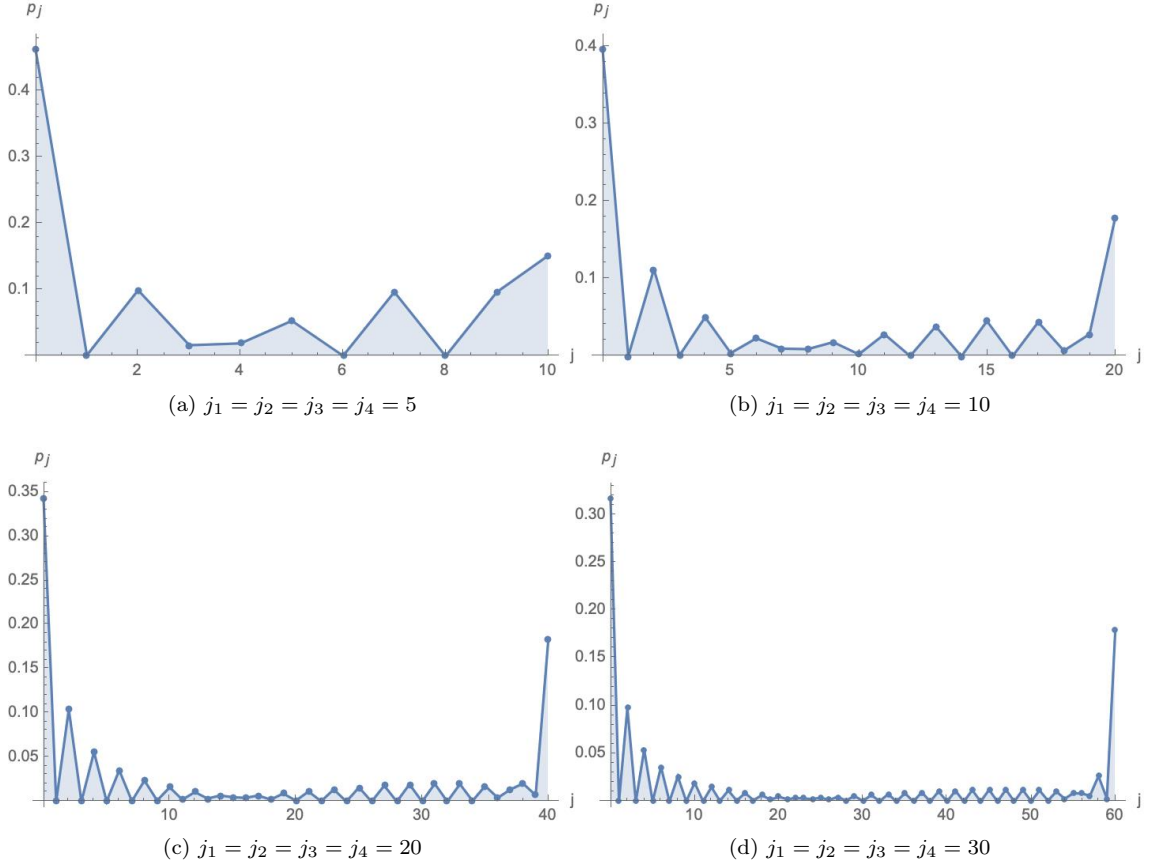


Figure 5: The numerical results of p_j for $(m_1, m_2, m_3, m_4) = (1, -1, 1, -1)$ and $j_1 = j_2 = j_3 = j_4 = 5, 10, 20, 30$, where the x -axis shows the recouping spin j and y -axis shows the numerical value of p_j . These figures show the difference in the shape of oscillation compared to the cases of $m_1 = m_2 = m_3 = m_4 = 0$.

3.3 Entanglement entropy between legs of coherent intertwiner

3.3.1 Coherent intertwiner with 4-legs

Let us consider the gauge invariant coherent intertwiner space $\mathcal{H}_v^{\{j_1, j_2, j_3, j_4\}} = \text{Inv}_{SU(2)}[V^{j_1} \otimes V^{j_2} \otimes \bar{V}^{j_3} \otimes \bar{V}^{j_4}]$ on a four-valents vertex, in which an element is given by

$$|\mathcal{I}\rangle = \int_{SU(2)} dg g|j_1, \hat{n}_1\rangle \otimes g|j_2, \hat{n}_2\rangle \otimes \langle j_3, \hat{n}_3|g^{-1} \otimes \langle j_4, \hat{n}_4|g^{-1}. \quad (46)$$

By recalling Eq.(11), the state is then rewritten in the manner of repeating Eq.(40) as illustrated in Fig.7, which reads

$$\begin{aligned} |\mathcal{I}\rangle &= \sum_{\vec{m}} c_{j_1, m_1}(\hat{n}_1) c_{j_2, m_2}(\hat{n}_2) \bar{c}_{j_3, m_3}(\hat{n}_3) \bar{c}_{j_4, m_4}(\hat{n}_4) \\ &\quad \cdot \int_{SU(2)} dg g|j_1, m_1\rangle \otimes |j_2, m_2\rangle \otimes \langle j_3, m_3| \otimes \langle j_4, m_4| g^{-1} \\ &= \sum_{\vec{m}} c_{j_1, m_1}(\hat{n}_1) c_{j_2, m_2}(\hat{n}_2) \bar{c}_{j_3, m_3}(\hat{n}_3) \bar{c}_{j_4, m_4}(\hat{n}_4) \sum_{j, m, k} \frac{\overline{C_{m_1 m_2 m}^{j_1 j_2 j}} C_{m_3 m_4 m}^{j_3 j_4 j}}{2j+1} |j_1, j_2; j, k\rangle \otimes \langle j_3, j_4; j, k|, \\ &= \sum_{j, m, k} \frac{C_{\hat{n}_1 \hat{n}_2 m}^{j_1 j_2 j} \overline{C_{\hat{n}_3 \hat{n}_4 m}^{j_3 j_4 j}}}{2j+1} |j_1, j_2; j, k\rangle \otimes \langle j_3, j_4; j, k| \end{aligned} \quad (48)$$

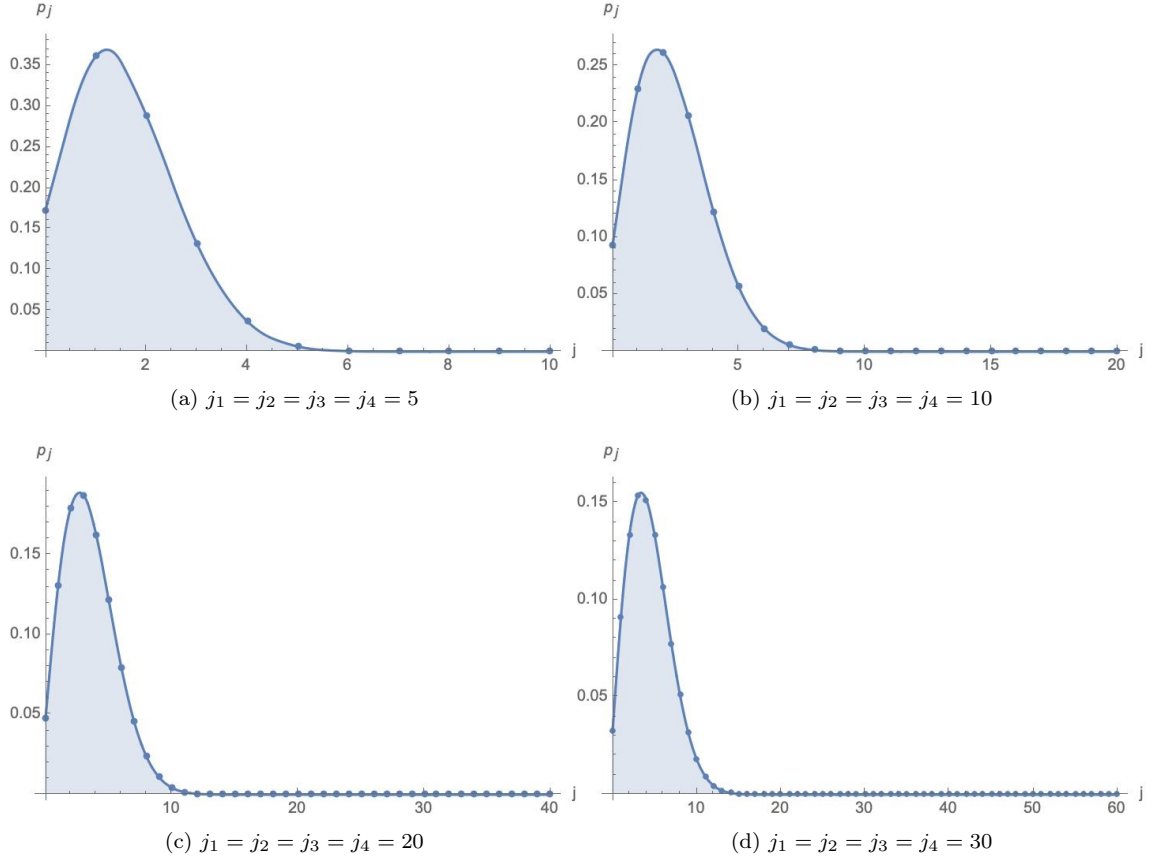


Figure 6: The numerical results of p_j for $j_1 = j_2 = j_3 = j_4 = 5, 10, 20, 30$ and $m_1 = m_3 = -m_2 = -m_4 = j_4$, where the x -axis shows the recoupling spin j and y -axis shows the numerical value of p_j . These figures show that the shape of the distributions p_j are peaks for the highest (and lowest) weight states.

(j_1, j_2, j_3, j_4)	(m_1, m_2, m_3, m_4)	$E_p(A B)$	$E_0(A B)$	$E(A B)$
(5, 5, 5, 5)	(0, 0, 0, 0)	1.58138	1.5931	3.17448
(5, 5, 5, 5)	(1, -1, 1, -1)	1.64349	1.37831	3.0218
(5, 5, 5, 5)	(2, -2, 2, -2)	1.68047	1.35532	3.03579
(5, 5, 5, 5)	(3, -3, 3, -3)	1.72176	1.33854	3.06029
(5, 5, 5, 5)	(4, -4, 4, -4)	1.6484	1.30671	2.95511
(5, 5, 5, 5)	(5, -5, 5, -5)	1.45701	1.21724	2.67426
(5, 5, 5, 5)	(2, -1, 2, -1)	1.7005	2.05912	3.75962
(5, 5, 5, 5)	(3, -1, 3, -1)	1.77649	2.32768	4.10417
(5, 5, 5, 5)	(4, -1, 4, -1)	1.59752	2.48947	4.08698
(5, 5, 5, 5)	(5, -1, 5, -1)	1.31356	2.60331	3.91687

Table 1: The numerical values of $E(A|B)$ for small spins $j_1 = j_2 = j_3 = j_4 = 5$ at different configurations with respect to magnetic numbers.

(j_1, j_2, j_3, j_4)	(m_1, m_2, m_3, m_4)	$E_p(A B)$	$E_0(A B)$	$E(A B)$
(10, 10, 10, 10)	(0, 0, 0, 0)	2.01747	2.02953	4.047
(10, 10, 10, 10)	(1, -1, 1, -1)	2.01367	1.80432	3.81799
(10, 10, 10, 10)	(2, -2, 2, -2)	2.06684	1.77726	3.8441
(10, 10, 10, 10)	(3, -3, 3, -3)	2.10459	1.76694	3.87153
(10, 10, 10, 10)	(4, -4, 4, -4)	2.1037	1.76034	3.86404
(10, 10, 10, 10)	(5, -5, 5, -5)	2.13296	1.75342	3.88638
(10, 10, 10, 10)	(6, -6, 6, -6)	2.16708	1.7438	3.91088
(10, 10, 10, 10)	(7, -7, 7, -7)	2.1329	1.72895	3.86185
(10, 10, 10, 10)	(8, -8, 8, -8)	2.08743	1.70467	3.7921
(10, 10, 10, 10)	(9, -9, 9, -9)	1.99391	1.66086	3.65477
(10, 10, 10, 10)	(10, -10, 10, -10)	1.77857	1.55688	3.33545

Table 2: The numerical values of $E(A|B)$ for small spins $j_1 = j_2 = j_3 = j_4 = 10$ at different configurations with respect to magnetic numbers.

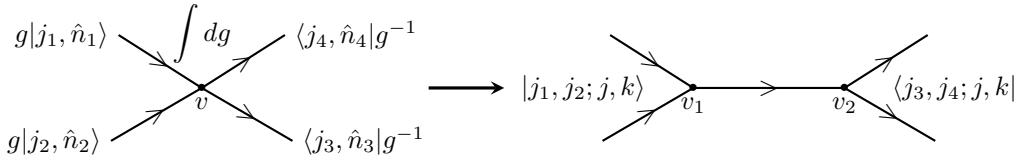


Figure 7: The $SU(2)$ -group-averaging on spin coherent state produces entanglement between the legs. This can be viewed as the entanglement between two coupled states $|j_1, j_2; j, k\rangle$ and $\langle j_3, j_4; j, k|$ at v_1 and v_2 , respectively.

where the second line uses the recoupled spins $|j_1, j_2; j, k\rangle := \sum_{m_1, m_2} C_{m_1 m_2 k}^{j_1 j_2 j} |j_1, m_1\rangle \otimes |j_2, m_2\rangle$ and $\langle j_3, j_4; j, k| := \sum_{m_3, m_4} \overline{C_{m_3 m_4 k}^{j_3 j_4 j}} \langle j_3, m_3| \otimes \langle j_4, m_4|$, and in the third line we have denoted

$$C_{\hat{n}_1 \hat{n}_2 m}^{j_1 j_2 j} \equiv \sum_{m_1=-j_1}^{j_1} \sum_{m_2=-j_2}^{j_2} c_{j_1, m_1}(\hat{n}_1) c_{j_2, m_2}(\hat{n}_2) \overline{C_{m_1 m_2 m}^{j_1 j_2 j}}, \quad (49)$$

$$\overline{C_{\hat{n}_3 \hat{n}_4 m}^{j_3 j_4 j}} \equiv \sum_{m_3=-j_3}^{j_3} \sum_{m_4=-j_4}^{j_4} \bar{c}_{j_3, m_3}(\hat{n}_3) \bar{c}_{j_4, m_4}(\hat{n}_4) C_{m_3 m_4 m}^{j_3 j_4 j}. \quad (50)$$

The density matrix of the coherent intertwiner $|\mathcal{I}\rangle$ is given by $\rho_{\mathcal{I}} \equiv \frac{|\mathcal{I}\rangle\langle\mathcal{I}|}{\langle\mathcal{I}|\mathcal{I}\rangle}$ where its denominator, namely, the normalization factor, is given by

$$\langle\mathcal{I}|\mathcal{I}\rangle = \sum_j \frac{1}{2j+1} \left| \sum_m C_{\hat{n}_1 \hat{n}_2 m}^{j_1 j_2 j} \overline{C_{\hat{n}_3 \hat{n}_4 m}^{j_3 j_4 j}} \right|^2. \quad (51)$$

Recall the definitions $\mathcal{H}_A := V^{j_1} \otimes V^{j_2}$ and $\mathcal{H}_B := \bar{V}^{j_3} \otimes \bar{V}^{j_4}$. Then, for the state $|\mathcal{I}\rangle$, the entanglement $E(A|B)$ between A and B can be given by the Von Neumann entropy of the reduced density matrices ρ_A , which are defined by

$$\rho_A := \text{Tr}_B(\rho_{\mathcal{I}}), \quad E(A|B) := -\text{Tr}(\rho_A \ln \rho_A). \quad (52)$$

More explicitly, ρ_A can be calculated as

$$\begin{aligned} \rho_A &= \text{Tr}_B(\rho_{\mathcal{I}}) \\ &= \sum_j \frac{1}{2j+1} \frac{\left| \sum_m C_{\hat{n}_1 \hat{n}_2 m}^{j_1 j_2 j} \overline{C_{\hat{n}_3 \hat{n}_4 m}^{j_3 j_4 j}} \right|^2}{\sum_{j'} \frac{1}{2j'+1} \left| \sum_{m'} C_{\hat{n}_1 \hat{n}_2 m'}^{j_1 j_2 j'} \overline{C_{\hat{n}_3 \hat{n}_4 m'}^{j_3 j_4 j'}} \right|^2} \sum_{k=-j}^j \frac{|j_1, j_2; j, k\rangle \langle j_1, j_2; j, k|}{2j+1}, \end{aligned} \quad (53)$$

which can be also read in the form of

$$\rho_A = \sum_j p_j \rho_j^A, \quad p_j = \frac{\left| \sum_m C_{\hat{n}_1 \hat{n}_2 m}^{j_1 j_2 j} \overline{C_{\hat{n}_3 \hat{n}_4 m}^{j_3 j_4 j}} \right|^2}{(2j+1) \left| \sum_{j', m} \frac{1}{2j'+1} C_{\hat{n}_1 \hat{n}_2 m'}^{j_1 j_2 j'} \overline{C_{\hat{n}_3 \hat{n}_4 m'}^{j_3 j_4 j'}} \right|^2}, \quad (54)$$

(j_1, j_2, j_3, j_4)	$(\theta_1, \theta_2, \theta_3, \theta_4)$	$(\varphi_1, \varphi_2, \varphi_3, \varphi_4)$	$E_p(A B)$	$E_0(A B)$	$E(A B)$
(5, 5, 5, 5)	$(\frac{\pi}{2}, \frac{\pi}{2}, \frac{\pi}{4}, \frac{3\pi}{4})$	$(0, \frac{\pi}{2}, \frac{\pi}{4}, \frac{\pi}{4})$	1.56229	2.70936	4.27165
(10, 10, 10, 10)	$(\frac{\pi}{2}, \frac{\pi}{2}, \frac{\pi}{4}, \frac{3\pi}{4})$	$(0, \frac{\pi}{2}, \frac{\pi}{4}, \frac{\pi}{4})$	1.8922	3.37298	5.26517
(15, 15, 15, 15)	$(\frac{\pi}{2}, \frac{\pi}{2}, \frac{\pi}{4}, \frac{3\pi}{4})$	$(0, \frac{\pi}{2}, \frac{\pi}{4}, \frac{\pi}{4})$	2.08976	3.76835	5.85811
(20, 20, 20, 20)	$(\frac{\pi}{2}, \frac{\pi}{2}, \frac{\pi}{4}, \frac{3\pi}{4})$	$(0, \frac{\pi}{2}, \frac{\pi}{4}, \frac{\pi}{4})$	2.23109	4.05092	6.28201
(25, 25, 25, 25)	$(\frac{\pi}{2}, \frac{\pi}{2}, \frac{\pi}{4}, \frac{3\pi}{4})$	$(0, \frac{\pi}{2}, \frac{\pi}{4}, \frac{\pi}{4})$	2.34114	4.271	6.61214
(30, 30, 30, 30)	$(\frac{\pi}{2}, \frac{\pi}{2}, \frac{\pi}{4}, \frac{3\pi}{4})$	$(0, \frac{\pi}{2}, \frac{\pi}{4}, \frac{\pi}{4})$	2.43131	4.45127	6.88258

Table 3: The numerical values of $E_p(A|B)$ and $E_0(A|B)$ for fixed $\hat{n}_1, \hat{n}_2, \hat{n}_3, \hat{n}_4$ and growth boundary spins. It is shown that $E_p(A|B)$ and $E_0(A|B)$ both grow with the boundary spins $j_1 = j_2 = j_3 = j_4$ getting larger.

(j_1, j_2, j_3, j_4)	$(\theta_1, \theta_2, \theta_3, \theta_4)$	$(\varphi_1, \varphi_2, \varphi_3, \varphi_4)$	$E_p(A B)$	$E_0(A B)$	$E(A B)$
(20, 20, 20, 20)	$(\frac{\pi}{2}, \frac{\pi}{2}, \frac{7\pi}{16}, \frac{9\pi}{16})$	$(0, \frac{\pi}{8}, \frac{\pi}{16}, \frac{\pi}{16})$	0.861644	4.38243	5.24407
(20, 20, 20, 20)	$(\frac{\pi}{2}, \frac{\pi}{2}, \frac{3\pi}{8}, \frac{5\pi}{8})$	$(0, \frac{\pi}{4}, \frac{\pi}{8}, \frac{\pi}{8})$	1.6089	4.3212	5.9301
(20, 20, 20, 20)	$(\frac{\pi}{2}, \frac{\pi}{2}, \frac{\pi}{4}, \frac{3\pi}{4})$	$(0, \frac{\pi}{2}, \frac{\pi}{4}, \frac{\pi}{4})$	2.23109	4.05092	6.28201
(20, 20, 20, 20)	$(\frac{\pi}{2}, \frac{\pi}{2}, \frac{\pi}{6}, \frac{5\pi}{6})$	$(0, \frac{2\pi}{3}, \frac{\pi}{3}, \frac{\pi}{3})$	2.43579	3.69809	6.13388
(20, 20, 20, 20)	$(\frac{\pi}{2}, \frac{\pi}{2}, \frac{\pi}{8}, \frac{7\pi}{8})$	$(0, \frac{3\pi}{4}, \frac{3\pi}{8}, \frac{3\pi}{8})$	2.50054	3.42048	5.92102
(20, 20, 20, 20)	$(\frac{\pi}{2}, \frac{\pi}{2}, \frac{\pi}{16}, \frac{13\pi}{16})$	$(0, \frac{7\pi}{8}, \frac{7\pi}{16}, \frac{7\pi}{16})$	2.541	2.65329	5.1943

Table 4: The numerical values of $E_p(A|B)$ and $E_0(A|B)$ for fixed boundary spins $j_1 = j_2 = j_3 = j_4 = 20$ and various angle $\arccos(\hat{n}_1 \cdot \hat{n}_2)$. It is shown that $E_p(A|B)$ increases while $E_0(A|B)$ decreases with the angle $\arccos(\hat{n}_1 \cdot \hat{n}_2)$ getting larger.

and $\rho_j^A = \frac{\sum_k |j_1, j_2; j, k\rangle \langle j_1, j_2; j, k|}{(2j+1)}$. Further, we have

$$E(A|B) = E_p(A|B) + E_0(A|B), \quad E_p(A|B) := - \sum_j (p_j \ln p_j), \quad E_0(A|B) := \sum_j p_j S_j^A \quad (55)$$

with $S_j^A \equiv -\text{Tr}(\rho_j^A \ln \rho_j^A) = \ln(2j+1)$.

One can see that $E(A|B)$ is determined by the distribution p_j . Generally, p_j is a rather complicated function of j for given $(j_1, \hat{n}_1, j_2, \hat{n}_2, j_3, \hat{n}_3, j_4, \hat{n}_4)$, thus it is hard to analyze the property of p_j by its analytical expression. We calculate p_j and $E(A|B)$ by the numerical methods as shown in Tab.3, Tab.4, Fig.8 and Fig.9. Our results shows that, p_j has a peak near $j = j_0 \equiv |j_1 \hat{n}_1 + j_2 \hat{n}_2|$. Especially, this peak shrinks relative to the range of j with the boundary spins j_1, j_2, j_3, j_4 getting larger, and this peak shrinks with the angle $\arccos(\hat{n}_1 \cdot \hat{n}_2)$ decreasing. Thus, we can argue that $E_0(A|B) = \sum_j p_j S_j^A \approx \ln(2j_0 + 1)$ reasonably. The term $E_p(A|B)$ is just the Shannon entropy of the distribution p_j . Note that the range $\max(|j_1 - j_2|, |j_3 - j_4|) \leq j \leq \min(|j_1 + j_2|, |j_3 + j_4|)$ of j grows linearly with j_1, j_2, j_3, j_4 going large. Then, based on the peakedness property of p_j , one can conclude that $E_p(A|B)$ increases no more than logarithmic growth with j_1, j_2, j_3, j_4 going large.

3.3.2 Coherent intertwiner with arbitrary number of legs

Let us consider the gauge invariant coherent intertwiner space $\mathcal{H}_v^{\{j, \tilde{j}\}} = \text{Inv}_{SU(2)}[\otimes_{I=1}^P V^{j_I} \otimes \otimes_{J=1}^Q \tilde{V}^{\tilde{j}_J}]$ on a $(P+Q)$ -valent vertex, in which an element is given by

$$|\mathcal{I}\rangle = \int_{SU(2)} dg \otimes_{I=1}^P g|j_I, \hat{n}_I\rangle \otimes_{J=1}^Q \langle \tilde{j}_J, \hat{n}_J | g^{-1}. \quad (56)$$

Similar to the coherent intertwiner with 4-legs, the coherent intertwiner with arbitrary number of legs can be expanded by the orthogonal re-coupling basis of intertwiner space, which reads

$$\begin{aligned} & |\mathcal{I}\rangle \\ &= \sum_j (2j+1) \left(\sum_{k, m=-j}^j |\mathcal{I}_P; j, m, k\rangle \langle \mathcal{I}_Q; j, m, k| \right) \\ &= \sum_j \sum_{j_{i_1}} \sum_{j_{i_2}} \dots \sum_{j_{i_p}} \sum_{\tilde{j}_{i_1}} \sum_{\tilde{j}_{i_2}} \dots \sum_{\tilde{j}_{i_q}} (2j+1)^{-1} \cdot c_{j, \tilde{j}_{i_1}, \tilde{j}_{i_2}}^{\mathcal{I}_P, \mathcal{I}_Q} \end{aligned} \quad (57)$$

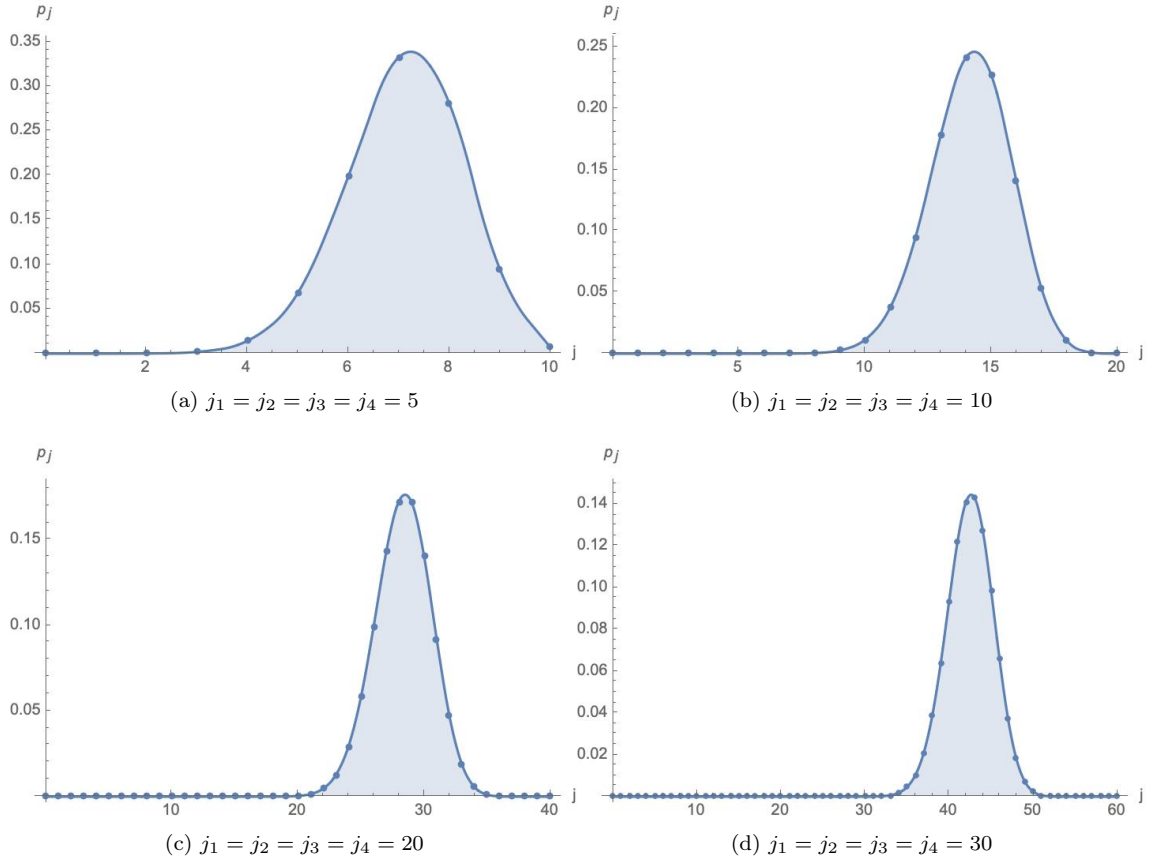


Figure 8: The numerical results of p_j for $(\theta_1, \theta_2, \theta_3, \theta_4) = (\frac{\pi}{2}, \frac{\pi}{2}, \frac{\pi}{4}, \frac{3\pi}{4}), (\varphi_1, \varphi_2, \varphi_3, \varphi_4) = (0, \frac{\pi}{2}, \frac{\pi}{4}, \frac{\pi}{4})$ and $j_1 = j_2 = j_3 = j_4 = 5, 10, 20, 30$, where the x -axis shows the recoupling spin j and y -axis shows the numerical value of p_j . These figures show that p_j has a peak near $j = j_0 \equiv |j_1 \hat{n}_1 + j_2 \hat{n}_2|$, and this peak shrinks relative to the range of j with the boundary spins j_1, j_2, j_3, j_4 getting larger.

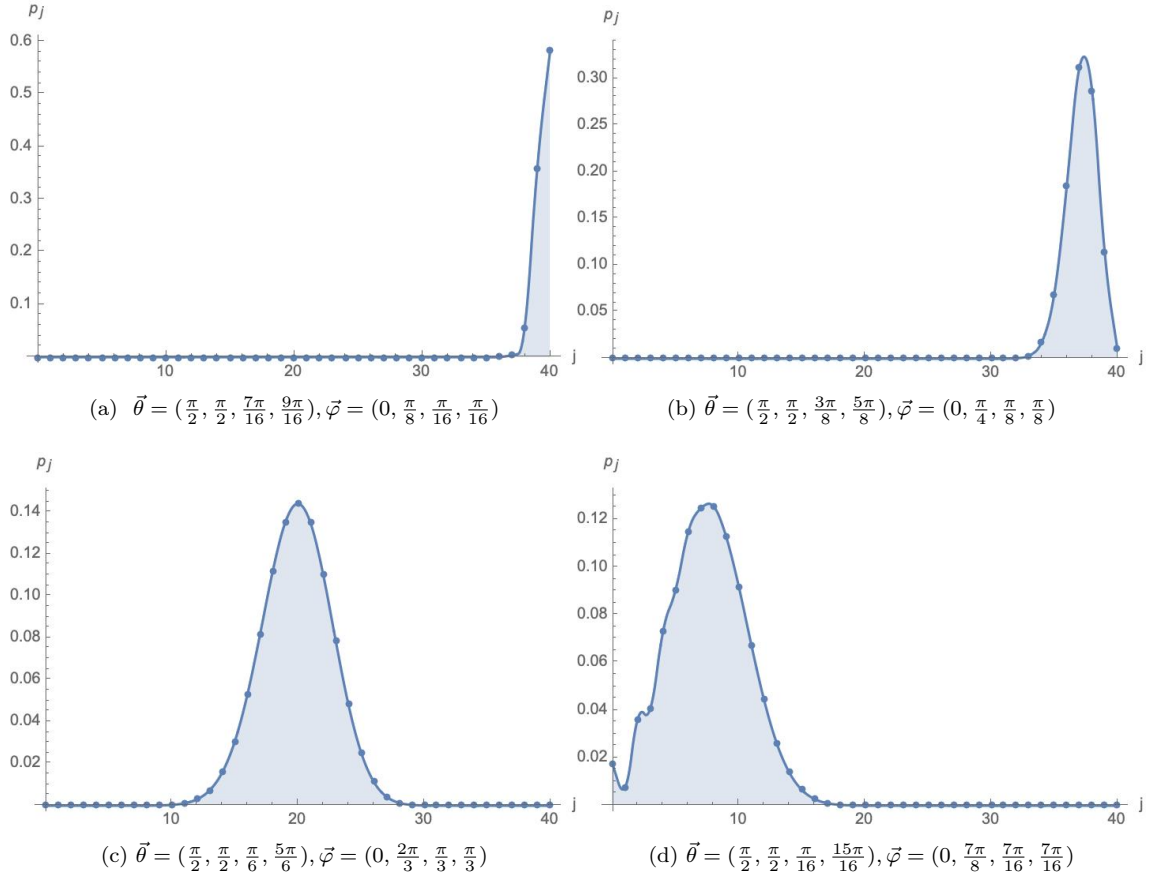


Figure 9: The numerical results of p_j for $j_1 = j_2 = j_3 = j_4 = 20$ and various $\vec{\theta} \equiv (\theta_1, \theta_2, \theta_3, \theta_4)$, $\vec{\varphi} \equiv (\varphi_1, \varphi_2, \varphi_3, \varphi_4)$, where the x -axis shows the recoupling spin j and y -axis shows the numerical value of p_j . These figures show that p_j has a peak near $j = j_0 \equiv |j_1 \hat{n}_1 + j_2 \hat{n}_2|$, and this peak shrinks with the angle $\arccos(\hat{n}_1 \cdot \hat{n}_2)$ decreasing.

$$\begin{aligned}
& \cdot \sum_k \sum_{k_{i_1}, \dots, k_{i_p}} \sum_{\tilde{k}_{i_1}, \dots, \tilde{k}_{i_q}} \left(|j_P, j_{P-1}; j_{i_p}, k_{i_p}\rangle \otimes |j_{i_p}, k_{i_p}; j_P; j_{i_{p-1}}, k_{i_{p-1}}\rangle \otimes \dots \right. \\
& \otimes |j_{i_2}, k_{i_2}; j_2; j_{i_1}, k_{i_1}\rangle \otimes |j_{i_1}, k_{i_1}; j_1; j, k\rangle \langle \tilde{j}_Q, \tilde{j}_{Q-1}; \tilde{j}_{i_q}, \tilde{k}_{i_q} | \otimes \langle \tilde{j}_{i_q}, \tilde{k}_{i_q}; \tilde{j}_q; \tilde{j}_{i_{q-1}}, \tilde{k}_{i_{q-1}} | \otimes \dots \\
& \left. \otimes \langle \tilde{j}_{i_2}, \tilde{k}_{i_2}; \tilde{j}_2; \tilde{j}_{i_1}, \tilde{k}_{i_1} | \otimes \langle \tilde{j}_{i_1}, \tilde{k}_{i_1}; \tilde{j}_1; j, k | \right),
\end{aligned}$$

where $|j', j''; j, k\rangle := \sum_{m', m''} C_{m' m'' k}^{j' j'' j} |j', m'\rangle \otimes |j'', m''\rangle$, $|j', k'; j'', j, k\rangle := \sum_{m''} C_{k' m'' k}^{j' j'' j} |j'', m''\rangle$, and $c_{j, \tilde{j}_i}^{\mathcal{I}_P, \mathcal{I}_Q}$ is the coefficient of this expansion, see the details in Appendix A.

Now, the density matrix of the coherent intertwiner $|\mathcal{I}\rangle$ can be given by $\rho_{\mathcal{I}} \equiv \frac{|\mathcal{I}\rangle\langle\mathcal{I}|}{\langle\mathcal{I}|\mathcal{I}\rangle}$. Let us define $\mathcal{H}_A := \otimes_{j=1}^P V^{j_I}$ and $\mathcal{H}_B := \otimes_{j=1}^Q \bar{V}^{\tilde{j}_j}$. Then, the entanglement $E(A|B)$ between A and B can be given by the Von Neumann entropy of the reduced density matrices ρ_A , which are defined as

$$\rho_A := \text{Tr}_B(\rho_{\mathcal{I}}), \quad E(A|B) := -\text{Tr}_A(\rho_A \ln \rho_A). \quad (58)$$

More explicitly, ρ_A can be calculated as

$$\rho_A = \text{Tr}_B(\rho_{\mathcal{I}}) = \frac{\text{Tr}_B(|\mathcal{I}\rangle\langle\mathcal{I}|)}{\langle\mathcal{I}|\mathcal{I}\rangle}, \quad (59)$$

where

$$\begin{aligned}
& \langle\mathcal{I}|\mathcal{I}\rangle \\
& = \sum_j \sum_{j_{i_1}, j_{i_2}, \dots, j_{i_p}} \sum_{\tilde{j}_{i_1}, \tilde{j}_{i_2}, \dots, \tilde{j}_{i_q}} (2j+1)^{-1} c_{j, \tilde{j}_i}^{\mathcal{I}_P, \mathcal{I}_Q} \overline{c_{j, \tilde{j}_i}^{\mathcal{I}_P, \mathcal{I}_Q}}.
\end{aligned} \quad (60)$$

and

$$\begin{aligned}
& \text{Tr}_B(|\mathcal{I}\rangle\langle\mathcal{I}|) \\
& = \sum_j \sum_{j_{i_1}, j_{i_2}, \dots, j_{i_p}} \sum_{j'_{i_1}, j'_{i_2}, \dots, j'_{i_p}} (2j+1)^{-1} \sum_{\tilde{j}_{i_1}, \tilde{j}_{i_2}, \dots, \tilde{j}_{i_q}} c_{j, \tilde{j}_i}^{\mathcal{I}_P, \mathcal{I}_Q} \overline{c_{j, \tilde{j}_i}^{\mathcal{I}_P, \mathcal{I}_Q}} \rho_{j, \tilde{j}_i}^A,
\end{aligned} \quad (61)$$

with

$$\begin{aligned}
\rho_{j, \tilde{j}_i}^A & := (2j+1)^{-1} \cdot \sum_k \sum_{k_{i_1}, \dots, k_{i_p}} \sum_{k'_{i_1}, \dots, k'_{i_p}} \left(|j_P, j_{P-1}; j_{i_p}, k_{i_p}\rangle \otimes |j_{i_p}, k_{i_p}; j_P; j_{i_{p-1}}, k_{i_{p-1}}\rangle \otimes \dots \right. \\
& \otimes |j_{i_2}, k_{i_2}; j_2; j_{i_1}, k_{i_1}\rangle \otimes |j_{i_1}, k_{i_1}; j_1; j, k\rangle \langle j_P, j_{P-1}; j'_{i_p}, k'_{i_p} | \otimes \langle j'_{i_p}, k'_{i_p}; j_P; j'_{i_{p-1}}, k'_{i_{p-1}} | \otimes \dots \\
& \left. \otimes \langle j'_{i_2}, k'_{i_2}; j_2; j'_{i_1}, k'_{i_1} | \otimes \langle j'_{i_1}, k'_{i_1}; j_1; j, k | \right).
\end{aligned} \quad (62)$$

It is direct to calculate that the Von Neumann entropy of ρ_{j, \tilde{j}_i}^A , which leads

$$S_j^A := -\text{Tr}_A(\rho_{j, \tilde{j}_i}^A \ln \rho_{j, \tilde{j}_i}^A) = \ln(2j+1). \quad (63)$$

Further, let us define

$$p_{j, \tilde{j}_i, j'_i} := \frac{(2j+1)^{-1} \sum_{\tilde{j}_{i_1}, \tilde{j}_{i_2}, \dots, \tilde{j}_{i_q}} c_{j, \tilde{j}_i}^{\mathcal{I}_P, \mathcal{I}_Q} \overline{c_{j, \tilde{j}_i}^{\mathcal{I}_P, \mathcal{I}_Q}}}{\langle\mathcal{I}|\mathcal{I}\rangle}, \quad (64)$$

$$\tilde{p}_j := \sum_{j_{i_1}, j_{i_2}, \dots, j_{i_p}} \sum_{j'_{i_1}, j'_{i_2}, \dots, j'_{i_p}} p_{j, \tilde{j}_i, j'_i}, \quad (65)$$

and

$$\bar{p}_{j, \tilde{j}_i, j'_i} := \frac{p_{j, \tilde{j}_i, j'_i}}{\tilde{p}_j}. \quad (66)$$

Then, the entanglement entropy $E(A|B)$ can be given by

$$E(A|B) = -\text{Tr}_A(\rho_A \ln \rho_A) = E_p(A|B) + \sum_j \tilde{p}_j \ln(2j+1) \quad (67)$$

where

$$\begin{aligned} E_p(A|B) &:= -\sum_j \sum_{j_{i_1}, j_{i_2}, \dots, j_{i_p}} \sum_{j'_{i_1}, j'_{i_2}, \dots, j'_{i_p}} (p_{j, j_i, j'_i} \ln p_{j, j_i, j'_i}) \\ &= -\sum_j \tilde{p}_j \ln \tilde{p}_j + \sum_j \tilde{p}_j E_{\tilde{p}_j}(A|B) \end{aligned} \quad (68)$$

with

$$E_{\tilde{p}_j}(A|B) := -\sum_{j_{i_1}, j_{i_2}, \dots, j_{i_p}} \sum_{j'_{i_1}, j'_{i_2}, \dots, j'_{i_p}} (\tilde{p}_{j, j_i, j'_i} \ln \tilde{p}_{j, j_i, j'_i}). \quad (69)$$

It is worth to have a discussion on this result. First, one can notice that $E(A|B)$ contains three terms $\sum_j \tilde{p}_j E_{\tilde{p}_j}(A|B)$, $\sum_j \tilde{p}_j \ln(2j+1)$ and $-\sum_j \tilde{p}_j \ln \tilde{p}_j$. This result takes a same formulation as the result (36) for the boundary entanglement of two entangled intertwiners. In fact, the recoupling edge labelled by spin j separates the coherent intertwiner as two entangled intertwiners, and the corresponding boundary entanglement of these two entangled intertwiners is given by $E(A|B)$ exactly, with $E_p(A|B)$ being the intertwiner entanglement and \tilde{p}_j being the probability distribution of the spin j on recoupling edge. Second, it is easy to see that the entanglement entropy $E(A|B)$ depends on the distribution $p_{j, j_i, \tilde{j}_i} = \tilde{p}_j \cdot \tilde{p}_{j, j_i, \tilde{j}_i}$ on the spins of the recoupling edges. In fact, by considering the peakedness property of coherent intertwiner, one can argue that p_{j, j_i, \tilde{j}_i} is peaked near the values

$$\begin{aligned} j_{i_p} &= |j_P \hat{n}_P + j_{P-1} \hat{n}_{P-1}|, & j_{i_{p-1}} &= |j_P \hat{n}_P + j_{P-1} \hat{n}_{P-1} + j_p \hat{n}_p|, & (70) \\ &\dots, & & & \\ j_{i_1} &= |j_P \hat{n}_P + j_{P-1} \hat{n}_{P-1} + j_p \hat{n}_p + \dots + j_2 \hat{n}_2|, & j &= |j_P \hat{n}_P + j_{P-1} \hat{n}_{P-1} + j_p \hat{n}_p + \dots + j_1 \hat{n}_1|, \\ \tilde{j}_{i_q} &= |\tilde{j}_Q \hat{n}_Q + \tilde{j}_{Q-1} \hat{n}_{Q-1}|, & \tilde{j}_{i_{q-1}} &= |\tilde{j}_Q \hat{n}_Q + \tilde{j}_{Q-1} \hat{n}_{Q-1} + \tilde{j}_q \hat{n}_q|, \\ &\dots, & & & \\ \tilde{j}_{i_1} &= |\tilde{j}_Q \hat{n}_Q + \tilde{j}_{Q-1} \hat{n}_{Q-1} + \tilde{j}_q \hat{n}_q + \dots + \tilde{j}_2 \hat{n}_2|, & \tilde{j} &= |\tilde{j}_Q \hat{n}_Q + \tilde{j}_{Q-1} \hat{n}_{Q-1} + \tilde{j}_q \hat{n}_q + \dots + \tilde{j}_1 \hat{n}_1|. \end{aligned}$$

This argument could be checked by evaluating the specific property of the distribution p_{j, j_i, \tilde{j}_i} . However, one can see that the general expression of p_{j, j_i, \tilde{j}_i} is too complicated to proceed the analytical study. One may also expect a numerical calculation of the distribution p_{j, j_i, \tilde{j}_i} , and we would like to leave this to future researches.

4 Conclusion and Outlook

To summarize, we focus on the entanglement between the legs of the intertwiners on vertices. We first review the relation between the boundary entanglement and intertwiner entanglement, and extend the result to the case that the internal edge carries a spin-superposition. Then, we turn to consider the specific intertwiners on a four-valents vertex, which is decomposed as two parts A and B attached by the labels $(j_1 m_1, j_2 m_2)$ and $(j_3 m_3, j_4 m_4)$ respectively. By introducing the group-averaging to the tensor-product type intertwiner on the four-valents vertex, we calculate the entanglement entropy $E(A|B)$ encoded in the group-averaged tensor-product intertwiner with various weights. The results show that, for the group-averaged tensor-product intertwiner with highest (and lowest) weight, the entanglement entropy is able to capture the main character of the probability distribution p_j of the recoupling spin j . This result suggests us to consider the entanglement entropy encoded in the gauge invariant coherent intertwiners. By introducing the recoupling edges to decompose the coherent intertwiner labelled by $(j_1 \hat{n}_1, j_2 \hat{n}_2)$ and $(j_3 \hat{n}_3, j_4 \hat{n}_4)$, we find that the entanglement is determined by the probability distribution p_j of the spins j on the recoupling edges of the coherent intertwiner, and the result of entanglement $E(A|B)$ is composed by the sum of two terms $E_p(A|B)$ and $E_0(A|B)$. The first term $E_p(A|B)$ is just the Shannon entropy of the distribution p_j , while the second term $E_0(A|B)$ is the expectation value of $\ln(2j+1)$ with respect to the distribution p_j . Our results show that, p_j has a peak near

$j = j_0 \equiv |j_1 \hat{n}_1 + j_2 \hat{n}_2|$; Especially, this peak shrinks relative to the range of j with the boundary spins j_1, j_2, j_3, j_4 getting larger, and this peak shrinks with the angle $\arccos(\hat{n}_1 \cdot \hat{n}_2)$ decreasing. Thus, we argue that $E_0(A|B) = \sum_j p_j S_j^A \approx \ln(2j_0 + 1)$, and the term $E_p(A|B)$ increases no more than logarithmic growth with j_1, j_2, j_3, j_4 going large. We also extend the analytical calculation part of entanglement to the case of gauge invariant coherent intertwiner on a $(P + Q)$ -valents vertex, which is also separated as two parts A and B attached by $(j_1, \hat{n}_1, j_2, \hat{n}_2, \dots, j_P, \hat{n}_P)$ and $(\tilde{j}_1, \hat{n}_1, \tilde{j}_2, \hat{n}_2, \dots, \tilde{j}_Q, \hat{n}_Q)$ respectively. By introducing the recoupling edges to decompose the gauge invariant coherent intertwiner, we give the probability distribution p_{j, j_i, \tilde{j}_i} of the spins j, j_i, \tilde{j}_i on the recoupling edges analytically, and show that the entanglement between A and B is determined by p_{j, j_i, \tilde{j}_i} .

It is worth to have some discussion on the results. First, one should notice that the entanglement entropy $E(A|B)$ are given based on the gauge invariant coherent intertwiners, which belong to the gauge invariant subspace of the total system $\mathcal{H}_A \otimes \mathcal{H}_B$. Thus, $E(A|B)$ describes the entanglement between some gauge invariant degrees of freedom, e.g. the face-angle $\theta = \arccos \hat{n}_1 \cdot \hat{n}_2$. However, the appearance of the factor $\ln(2j + 1)$ comes from breaking the gauge invariance, and the physical meaning of the factor $\ln(2j + 1)$ depends on how to define boundaries at the quantum level for non-Abelian lattice gauge theories and LQG [37]. Second, the entanglement between the legs of coherent intertwiner can be related to the face-angle of the semiclassical polyhedron. Recall that p_j has a peak near $j_0 \equiv |j_1 \hat{n}_1 + j_2 \hat{n}_2|$ and this peak shrinks with the angle $\arccos(\hat{n}_1 \cdot \hat{n}_2)$ decreasing. Thus, the Shannon entropy $E_p(A|B)$ of the distribution p_j decreases with the face-angle $\pi - \arccos(\hat{n}_1 \cdot \hat{n}_2)$ increasing. Nevertheless, one also note that another term $E_0(A|B) \approx \ln(2j_0 + 1)$ in $E(A|B)$ increases with the face-angle $\pi - \arccos(\hat{n}_1 \cdot \hat{n}_2)$ increasing. Hence, the entanglement $E(A|B)$ may not have monotonous dependency on the face-angle $\pi - \arccos(\hat{n}_1 \cdot \hat{n}_2)$, e.g. as shown in Tab.4, $E(A|B)$ increases first and then decreases with the face-angle $\pi - \arccos(\hat{n}_1 \cdot \hat{n}_2)$ increasing for $j_1 = j_2 = j_3 = j_4 = 20$. Third, we would like to emphasis that the entanglement on the two-vertices graph with one link is independent on holonomy-insertion [37]. In other words, the holonomy living along the edge connecting these two vertices is irrelevant to the entanglement entropy at all. This property is attributed to the observation that the holonomy can be eliminated by a boundary unitary. This implies that the entanglement do not distinguish between a two-vertex graph and its coarse-grained graph (single vertex) provided that there is only one link. For the cases of two-vertices graph with multi-links, the nontrivial loop is introduced, which should be viewed as excitation of gauge curvature [50, 51], or interpreted as topological defect [52–54]. The related studies of entanglement for the cases can be found in [39, 54]. As for the entanglement in coherent states admitting gauge curvature, we leave the exploration in the future.

It is also worth to have an outlook on the use of entanglement in the study of black hole entropy in the framework of loop quantum gravity [55–60]. A typical method for statistics of black holes in loop quantum gravity is to consider the classical boundary conditions for isolated horizons [55, 57]. This boundary theory is given as a Chern-Simons theory and the horizon is described as a classical surface punctured by the edges of spin-network states. Then, the black hole entropy is calculated by counting the Chern-Simons states for a punctured sphere. This picture could also be considered in the full theory of LQG. We would have the horizon cutting the spin-networks, and the entanglement entropy between the black hole interior and exterior comes directly from the contributions of all the punctures on the horizon [32, 61]. In fact, these punctures can be generated by the edges or true vertices of the spin-networks crossing the horizon. It has been argued that the puncture generated by an edge crossing the horizon contributes the boundary spin state entanglement to the entanglement entropy between the black hole interior and exterior [37]. Nevertheless, the space-time geometry near the horizon of a massive Schwarzschild black hole should be described by the semi-classical state in LQG, which could not only control the classical property of horizon but also admit the quantum perturbation to generate the Hawking radiation. Thus, it seems inevitable that the coherent states on graphs and coherent intertwiners on vertices would control the entanglement contribution of the punctures generated by the edges or true vertices crossing the horizon. Our studies in this paper provides a basement to explore the entanglement contribution coming from coherent intertwiners, and it can be extended to study the the entanglement contribution coming from coherent states on graphs (e.g., Thiemann’s coherent state and twisted geometry coherent state [27–30, 40–43]).

Acknowledgments

This work is supported by the project funded by the National Natural Science Foundation of China (NSFC) with Grants No. 12047519 and No. 12165005. G. L. is supported by “the Fundamental Research Funds for the Central Universities”. Q. C. is funded within the QUANTERA II Programme that has received funding from the European Union’s Horizon 2020 research and innovation programme under Grant Agreement No 101017733 (VERIQTAS).

A The re-coupling expansion of coherent intertwiner with arbitrary number of legs

By introduce a recoupling edge labelled by spin j , the coherent intertwiner $|\mathcal{I}\rangle$ can be decomposed as

$$\begin{aligned}
|\mathcal{I}\rangle &= \int_{SU(2)} dg \bigotimes_{I=1}^P g|j_I, \hat{n}_I\rangle \int_{SU(2)} dh \delta(g^{-1}h) \bigotimes_{J=1}^Q \langle \tilde{j}_J, \hat{n}_J | h^{-1} \\
&= \sum_j (2j+1) \int_{SU(2)} dg \int_{SU(2)} dh \bigotimes_{I=1}^P g|j_I, \hat{n}_I\rangle \text{tr}^j(g^{-1}h) \bigotimes_{J=1}^Q \langle \tilde{j}_J, \hat{n}_J | h^{-1} \\
&= \sum_j (2j+1) \left(\sum_{m,k=-j}^j \int_{SU(2)} dg \bigotimes_{I=1}^P g|j_I, \hat{n}_I\rangle \otimes \langle j, m | g^{-1} | j, k\rangle \otimes \int_{SU(2)} dh \langle j, k | h | j, m\rangle \bigotimes_{J=1}^Q \langle \tilde{j}_J, \hat{n}_J | h^{-1} \right) \\
&= \sum_j (2j+1) \left(\sum_{m,k=-j}^j |\mathcal{I}_P; j, m, k\rangle \langle \mathcal{I}_Q; j, m, k| \right),
\end{aligned} \tag{71}$$

where

$$\begin{aligned}
|\mathcal{I}_P; j, m, k\rangle &:= \int_{SU(2)} dg \bigotimes_{I=1}^P g|j_I, \hat{n}_I\rangle \otimes \langle j, m | g^{-1} | j, k\rangle, \\
\langle \mathcal{I}_Q; j, m, k| &:= \int_{SU(2)} dh \langle j, k | h | j, m\rangle \bigotimes_{J=1}^Q \langle \tilde{j}_J, \hat{n}_J | h^{-1}
\end{aligned} \tag{72}$$

are projectors that send tensor representations to recoupling representations, see the illustration in Fig.10.

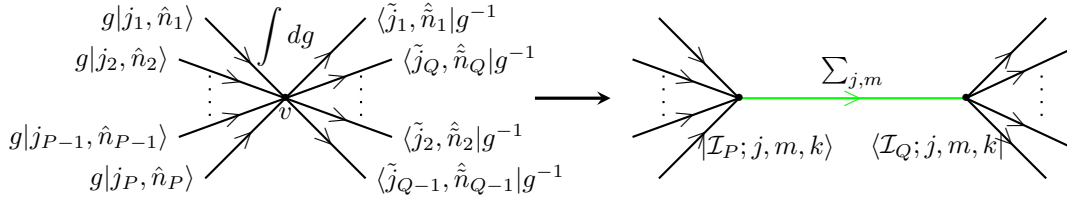


Figure 10: The illustration of recoupling spin j for \mathcal{I} .

One can further insert recoupling edges adapting to a recoupling scheme for $|\mathcal{I}_P, j, m\rangle$ step by step. Following the re-coupling scheme illustrated in Fig.11 and using character formula for delta function

$$\begin{aligned}
g|jm\rangle \otimes \langle j'm'|g^{-1} &= \int_{SU(2)} dh \delta(g^{-1}h) h|jm\rangle \otimes \langle j'm'|h^{-1} \\
&= \sum_{j''} (2j''+1) \int_{SU(2)} dh \text{tr}^{j''}(hg^{-1}) h|jm\rangle \otimes \langle j'm'|h^{-1},
\end{aligned}$$

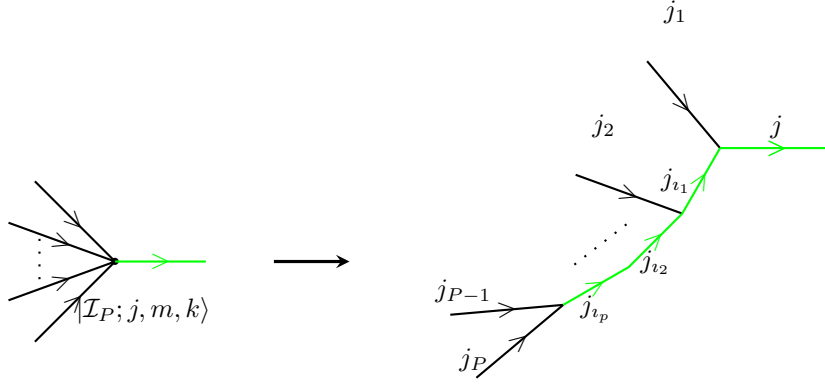


Figure 11: The illustration of recoupling spins for $|\mathcal{I}_P; j, m, k\rangle$.

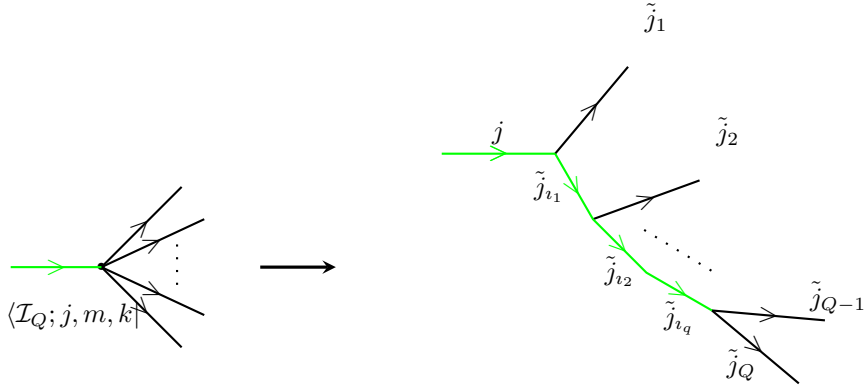


Figure 12: The illustration of recoupling spins for $\langle \mathcal{I}_Q; j, m, k|$.

one can get

$$\begin{aligned}
|\mathcal{I}_P; j, m, k\rangle &:= \int_{SU(2)} dg \left(\bigotimes_{I=1}^P g |j_I, \hat{n}_I\rangle \right) \otimes \langle j, m | g^{-1} |j, k\rangle \quad (73) \\
&= \sum_{j_{i_1}} (2j_{i_1} + 1) \sum_{m_{i_1}, k_{i_1} = -j_{i_1}}^{j_{i_1}} \int_{SU(2)} dg \bigotimes_{I=2}^P g |j_I, \hat{n}_I\rangle \cdot \langle j_{i_1}, m_{i_1} | g^{-1} |j_{i_1}, k_{i_1}\rangle \otimes |j_{i_1} k_{i_1} m_{i_1}, j_1 \hat{n}_1, j m k\rangle \\
&= \sum_{j_{i_1}} \sum_{j_{i_2}} (2j_{i_1} + 1)(2j_{i_2} + 1) \left(\sum_{m_{i_1}, k_{i_1} = -j_{i_1}}^{j_{i_1}} \sum_{m_{i_2}, k_{i_2} = -j_{i_2}}^{j_{i_2}} \int_{SU(2)} dg \bigotimes_{I=3}^P g |j_I, \hat{n}_I\rangle \cdot \langle j_{i_2}, m_{i_2} | g^{-1} |j_{i_2}, k_{i_2}\rangle \right. \\
&\quad \left. \otimes |j_{i_2} k_{i_2} m_{i_2}, j_2 \hat{n}_2, j_{i_1} m_{i_1} k_{i_1}\rangle \otimes |j_{i_1} k_{i_1} m_{i_1}, j_1 \hat{n}_1, j m k\rangle \right) \\
&= \sum_{j_{i_1}} \sum_{j_{i_2}} \dots \sum_{j_{i_p}} (2j_{i_1} + 1)(2j_{i_2} + 1) \dots (2j_{i_p} + 1) \\
&\quad \cdot \left(\sum_{m_{i_1}, k_{i_1} = -j_{i_1}}^{j_{i_1}} \sum_{m_{i_2}, k_{i_2} = -j_{i_2}}^{j_{i_2}} \dots \sum_{m_{i_p}, k_{i_p} = -j_{i_p}}^{j_{i_p}} |j_P \hat{n}_P, j_{P-1} \hat{n}_{P-1}, j_{i_p} m_{i_p} k_{i_p}\rangle \right. \\
&\quad \left. \otimes |j_{i_p} k_{i_p} m_{i_p}, j_P \hat{n}_P, j_{i_{p-1}} m_{i_{p-1}} k_{i_{p-1}}\rangle \otimes \dots \otimes |j_2 k_2 m_2, j_2 \hat{n}_2, j_{i_1} m_{i_1} k_{i_1}\rangle \otimes |j_{i_1} k_{i_1} m_{i_1}, j_1 \hat{n}_1, j m k\rangle \right) \\
&= \sum_{j_{i_1}} \sum_{j_{i_2}} \dots \sum_{j_{i_p}} (2j + 1)^{-1}
\end{aligned}$$

$$\cdot \sum_{m_{i_1}, k_{i_1} = -j_{i_1}}^{j_{i_1}} \sum_{m_{i_2}, k_{i_2} = -j_{i_2}}^{j_{i_2}} \cdots \sum_{m_{i_p}, k_{i_p} = -j_{i_p}}^{j_{i_p}} c_{\hat{n}_P, \hat{n}_{P-1}, m_{i_p}}^{j_P, j_{P-1}, j_{i_p}} c_{m_{i_p}, \hat{n}_p, m_{i_{p-1}}}^{j_{i_p}, j_p, j_{i_{p-1}}} \cdots c_{m_{i_2}, \hat{n}_2, m_{i_1}}^{j_{i_2}, j_2, j_{i_1}} c_{m_{i_1}, \hat{n}_1, m}^{j_{i_1}, j_1, j} \cdot \left(|j_P, j_{P-1}; j_{i_p}, k_{i_p}\rangle \otimes |j_{i_p}, k_{i_p}; j_p; j_{i_{p-1}}, k_{i_{p-1}}\rangle \otimes \cdots \otimes |j_{i_2}, k_{i_2}; j_2; j_{i_1}, k_{i_1}\rangle \otimes |j_{i_1}, k_{i_1}; j_1; j, k\rangle \right)$$

with $p := P - 2$, where we defined

$$c_{m_{i_1}, \hat{n}_1, m}^{j_{i_1}, j_1, j} := \sum_{k'_{i_1} = -j_{i_1}}^{j_{i_1}} \sum_{k' = -j}^j \langle j_{i_1}, k'_{i_1}; j_1; j, k' | j_{i_1} k'_{i_1} m_{i_1}, j_1 \hat{n}_1, j m k' \rangle, \quad (74)$$

$$c_{m_{i_2}, \hat{n}_2, m_{i_1}}^{j_{i_2}, j_2, j_{i_1}} := \sum_{k'_{i_2} = -j_{i_2}}^{j_{i_2}} \sum_{k'_{i_1} = -j_{i_1}}^{j_{i_1}} \langle j_{i_2}, k'_{i_2}; j_2; j_{i_1}, k_{i_1} | j_{i_2} k'_{i_2} m_{i_2}, j_2 \hat{n}_2, j_{i_1} m_{i_1} k'_{i_1} \rangle, \quad (75)$$

$$\cdots, \quad (76)$$

$$c_{\hat{n}_P, \hat{n}_{P-1}, m_{i_p}}^{j_P, j_{P-1}, j_{i_p}} := \sum_{k'_{i_p} = -j_{i_p}}^{j_{i_p}} \langle j_P, j_{P-1}; j_{i_p}, k'_{i_p} | j_P \hat{n}_P, j_{P-1} \hat{n}_{P-1}, j_{i_p} m_{i_p} k'_{i_p} \rangle, \quad (77)$$

and

$$|j_{i_1} k'_{i_1} m_{i_1}, j_1 \hat{n}_1, j m k'\rangle := \int_{SU(2)} dg g |j_1, \hat{n}_1\rangle \langle j_{i_1} k'_{i_1} | g |j_{i_1}, m_{i_1}\rangle \cdot \langle j, m | g^{-1} |j, k'\rangle, \quad (78)$$

$$|j_{i_2} k'_{i_2} m_{i_2}, j_2 \hat{n}_2, j_{i_1} m_{i_1} k'_{i_1}\rangle := \int_{SU(2)} dg g |j_2, \hat{n}_2\rangle \langle j_{i_2}, k'_{i_2} | g |j_{i_2}, m_{i_2}\rangle \cdot \langle j_{i_1} m_{i_1} | g^{-1} |j_{i_1}, k'_{i_1}\rangle, \quad (79)$$

$$\cdots, \quad (80)$$

$$|j_P \hat{n}_P, j_{P-1} \hat{n}_{P-1}, j_{i_p} m_{i_p} k'_{i_p}\rangle := \int_{SU(2)} dg g |j_P, \hat{n}_P\rangle \otimes g |j_{P-1}, \hat{n}_{P-1}\rangle \langle j_{i_p}, m_{i_p} | g^{-1} |j_{i_p}, k'_{i_p}\rangle \quad (81)$$

with $|j', j''; j, k\rangle := \sum_{m', m''} C_{m' m'' k}^{j' j'' j} |j', m'\rangle \otimes |j'', m''\rangle$, $|j', k'; j'', j, k\rangle := \sum_{m''} C_{k' m'' k}^{j' j'' j} |j'', m''\rangle$. Similarly, as the illustration in Fig.12, one can expand

$$\begin{aligned} \langle \mathcal{I}_Q; j, m, k | &:= \int_{SU(2)} dh \langle j, k | h | j, m \rangle \bigotimes_{J=1}^Q \langle \tilde{j}_J, \hat{n}_J | h^{-1} \\ &= \sum_{\tilde{j}_{i_1}} (2\tilde{j}_{i_1} + 1) \left(\sum_{\tilde{m}_{i_1}, \tilde{k}_{i_1} = -\tilde{j}_{i_1}}^{\tilde{j}_{i_1}} \int_{SU(2)} dh \langle \tilde{j}_{i_1}, \tilde{k}_{i_1} | h | \tilde{j}_{i_1}, \tilde{m}_{i_1} \rangle \bigotimes_{J=2}^Q \langle \tilde{j}_J, \hat{n}_J | h^{-1} \otimes \langle \tilde{j}_{i_1} \tilde{m}_{i_1} \tilde{k}_{i_1}, \tilde{j}_1 \hat{n}_1, j k m | \right) \\ &= \sum_{\tilde{j}_{i_1}} \sum_{\tilde{j}_{i_2}} \cdots \sum_{\tilde{j}_{i_q}} (2\tilde{j}_{i_q} + 1)^{-1} \\ &\cdot \sum_{\tilde{m}_{i_1}, \tilde{k}_{i_1} = -\tilde{j}_{i_1}}^{\tilde{j}_{i_1}} \sum_{\tilde{m}_{i_2}, \tilde{k}_{i_2} = -\tilde{j}_{i_2}}^{\tilde{j}_{i_2}} \cdots \sum_{\tilde{m}_{i_q}, \tilde{k}_{i_q} = -\tilde{j}_{i_q}}^{\tilde{j}_{i_q}} c_{\hat{n}_Q, \hat{n}_{Q-1}, \tilde{m}_{i_q}}^{\tilde{j}_Q, \tilde{j}_{Q-1}, \tilde{j}_{i_q}} c_{\tilde{m}_{i_q}, \hat{n}_q, \tilde{m}_{i_{q-1}}}^{\tilde{j}_{i_q}, \tilde{j}_q, \tilde{j}_{i_{q-1}}} \cdots c_{\tilde{m}_{i_2}, \hat{n}_2, \tilde{m}_{i_1}}^{\tilde{j}_{i_2}, \tilde{j}_2, \tilde{j}_{i_1}} c_{\tilde{m}_{i_1}, \hat{n}_1, m}^{\tilde{j}_{i_1}, \tilde{j}_1, j} \\ &\cdot \left(\langle \tilde{j}_Q, \tilde{j}_{Q-1}; \tilde{j}_{i_q}, \tilde{k}_{i_q} | \otimes \langle \tilde{j}_{i_q}, \tilde{k}_{i_q}; \tilde{j}_q; \tilde{j}_{i_{q-1}}, \tilde{k}_{i_{q-1}} | \otimes \cdots \otimes \langle \tilde{j}_{i_2}, \tilde{k}_{i_2}; \tilde{j}_2; \tilde{j}_{i_1}, \tilde{k}_{i_1} | \otimes \langle \tilde{j}_{i_1}, \tilde{k}_{i_1}; \tilde{j}_1; j, k | \right) \end{aligned} \quad (82)$$

with $q = Q - 2$, where we defined

$$c_{\tilde{m}_{i_1}, \hat{n}_1, m}^{\tilde{j}_{i_1}, \tilde{j}_1, j} := \sum_{\tilde{k}'_{i_1}, k'} \langle \tilde{j}_{i_1} \tilde{m}_{i_1} \tilde{k}'_{i_1}, \tilde{j}_1 \hat{n}_1, j k' m | \tilde{j}_{i_1}, \tilde{k}'_{i_1}; \tilde{j}_1; j, k' \rangle, \quad (83)$$

$$c_{\tilde{m}_{i_2}, \tilde{\hat{n}}_2, \tilde{m}_{i_1}}^{\tilde{j}_{i_2}, \tilde{j}_2, \tilde{j}_{i_1}} := \sum_{\tilde{k}'_1, \tilde{k}'_2} \langle \tilde{j}_{i_2} \tilde{m}_{i_2} \tilde{k}'_2, \tilde{j}_2 \tilde{\hat{n}}_2, \tilde{j}_{i_1} \tilde{k}'_1 \tilde{m}_{i_1} | \tilde{j}_{i_2}, \tilde{k}'_2; \tilde{j}_2; \tilde{j}_{i_1}, \tilde{k}'_1 \rangle, \quad (84)$$

$$\dots, \quad (85)$$

$$c_{\tilde{\hat{n}}_Q, \tilde{\hat{n}}_{Q-1}, \tilde{m}_{i_q}}^{\tilde{j}_Q, \tilde{j}_{Q-1}, \tilde{j}_{i_q}} := \sum_{\tilde{k}'_q} \langle \tilde{j}_Q \tilde{\hat{n}}_Q, \tilde{j}_{Q-1} \tilde{\hat{n}}_{Q-1}, \tilde{j}_{i_q} \tilde{k}'_q \tilde{m}_{i_q} | \tilde{j}_Q, \tilde{j}_{Q-1}; \tilde{j}_{i_q}, \tilde{k}'_q \rangle, \quad (86)$$

and

$$\langle \tilde{j}_{i_1} \tilde{m}_{i_1} \tilde{k}'_1, \tilde{j}_1 \tilde{\hat{n}}_1, j k' m | := \int_{SU(2)} dg \otimes \langle j, k' | g | j, m \rangle \langle \tilde{j}_{i_1}, \tilde{m}_{i_1} | g^{-1} | \tilde{j}_{i_1}, \tilde{k}'_1 \rangle \otimes \langle \tilde{j}_1, \tilde{\hat{n}}_1 | g^{-1}, \quad (87)$$

$$\langle \tilde{j}_{i_2} \tilde{m}_{i_2} \tilde{k}'_2, \tilde{j}_2 \tilde{\hat{n}}_2, \tilde{j}_{i_1} \tilde{k}'_1 \tilde{m}_{i_1} | := \int_{SU(2)} dg \langle \tilde{j}_{i_1}, \tilde{k}'_1 | g | \tilde{j}_{i_1}, \tilde{m}_{i_1} \rangle \langle \tilde{j}_{i_2}, \tilde{m}_{i_2} | g^{-1} | \tilde{j}_{i_2}, \tilde{k}'_2 \rangle \otimes \langle \tilde{j}_2, \tilde{\hat{n}}_2 | g^{-1}, \quad (88)$$

$$\dots, \quad (89)$$

$$\langle \tilde{j}_Q \tilde{\hat{n}}_Q, \tilde{j}_{Q-1} \tilde{\hat{n}}_{Q-1}, \tilde{j}_{i_q} \tilde{k}'_q \tilde{m}_{i_q} | := \int_{SU(2)} dg \langle \tilde{j}_{i_q}, \tilde{k}'_q | g | \tilde{j}_{i_q}, \tilde{m}_{i_q} \rangle \langle \tilde{j}_Q, \tilde{\hat{n}}_Q | g^{-1} \otimes \langle \tilde{j}_{Q-1}, \tilde{\hat{n}}_{Q-1} | g^{-1}. \quad (90)$$

Then, one has

$$\begin{aligned} & |\mathcal{I}\rangle \\ &= \sum_j (2j+1) \left(\sum_{m, k=-j}^j |\mathcal{I}_P; j, m, k\rangle \langle \mathcal{I}_Q; j, m, k| \right) \\ &= \sum_j \sum_{j_{i_1}} \sum_{j_{i_2}} \dots \sum_{j_{i_p}} \sum_{\tilde{j}_{i_1}} \sum_{\tilde{j}_{i_2}} \dots \sum_{\tilde{j}_{i_q}} (2j+1)^{-1} \\ &\quad \cdot c_{j, j_i, \tilde{j}_i}^{\mathcal{I}_P, \mathcal{I}_Q} \cdot \sum_{k=-j}^j \sum_{\tilde{k}_{i_1}=-\tilde{j}_{i_1}}^{\tilde{j}_{i_1}} \sum_{\tilde{k}_{i_2}=-\tilde{j}_{i_2}}^{\tilde{j}_{i_2}} \dots \sum_{\tilde{k}_{i_q}=-\tilde{j}_{i_q}}^{\tilde{j}_{i_q}} \sum_{k_{i_1}=-j_{i_1}}^{j_{i_1}} \sum_{k_{i_2}=-j_{i_2}}^{j_{i_2}} \dots \sum_{k_{i_p}=-j_{i_p}}^{j_{i_p}} \left(|\mathcal{I}_P, j_{P-1}; j_{i_p}, k_{i_p}\rangle \right. \\ &\quad \otimes |j_{i_p}, k_{i_p}; j_p; j_{i_{p-1}}, k_{i_{p-1}}\rangle \otimes \dots \otimes |j_{i_2}, k_{i_2}; j_2; j_{i_1}, k_{i_1}\rangle \otimes |j_{i_1}, k_{i_1}; j_1; j, k\rangle \langle \tilde{j}_Q, \tilde{j}_{Q-1}; \tilde{j}_{i_q}, \tilde{k}_{i_q}| \\ &\quad \left. \otimes \langle \tilde{j}_{i_q}, \tilde{k}_{i_q}; \tilde{j}_q; \tilde{j}_{i_{q-1}}, \tilde{k}_{i_{q-1}}| \otimes \dots \otimes \langle \tilde{j}_{i_2}, \tilde{k}_{i_2}; \tilde{j}_2; \tilde{j}_{i_1}, \tilde{k}_{i_1}| \otimes \langle \tilde{j}_{i_1}, \tilde{k}_{i_1}; \tilde{j}_1; j, k| \right), \end{aligned} \quad (91)$$

where

$$\begin{aligned} & c_{j, j_i, \tilde{j}_i}^{\mathcal{I}_P, \mathcal{I}_Q} \\ &:= \sum_{m=-j}^j \sum_{\tilde{m}_{i_1}=-\tilde{j}_{i_1}}^{\tilde{j}_{i_1}} \sum_{\tilde{m}_{i_2}=-\tilde{j}_{i_2}}^{\tilde{j}_{i_2}} \dots \sum_{\tilde{m}_{i_q}=-\tilde{j}_{i_q}}^{\tilde{j}_{i_q}} \sum_{m_{i_1}=-j_{i_1}}^{j_{i_1}} \sum_{m_{i_2}=-j_{i_2}}^{j_{i_2}} \dots \sum_{m_{i_p}=-j_{i_p}}^{j_{i_p}} c_{\tilde{\hat{n}}_Q, \tilde{\hat{n}}_{Q-1}, \tilde{m}_{i_q}}^{\tilde{j}_Q, \tilde{j}_{Q-1}, \tilde{j}_{i_q}} \\ &\quad \cdot c_{\tilde{m}_{i_q}, \tilde{\hat{n}}_q, \tilde{m}_{i_{q-1}}}^{\tilde{j}_{i_q}, \tilde{j}_q; \tilde{j}_{i_{q-1}}} \dots c_{\tilde{m}_{i_2}, \tilde{\hat{n}}_2, \tilde{m}_{i_1}}^{\tilde{j}_{i_2}, \tilde{j}_2; \tilde{j}_{i_1}} c_{\tilde{m}_{i_1}, \tilde{\hat{n}}_1, m}^{\tilde{j}_{i_1}, \tilde{j}_1; j} c_{\tilde{\hat{n}}_P, \tilde{\hat{n}}_{P-1}, m_{i_p}}^{j_P, j_{P-1}, j_{i_p}} c_{m_{i_p}, \tilde{\hat{n}}_p, m_{i_{p-1}}}^{j_{i_p}, j_p; j_{i_{p-1}}} \dots c_{m_{i_2}, \tilde{\hat{n}}_2, m_{i_1}}^{j_{i_2}, j_2; j_{i_1}} c_{m_{i_1}, \tilde{\hat{n}}_1, m}^{j_{i_1}, j_1; j}. \end{aligned} \quad (92)$$

References

- [1] A. Ashtekar and J. Pullin, *Loop quantum gravity: The first 30 years*. World Scientific Publishing Co. Pte Ltd, Singapore, Mar., 2017.
- [2] A. Ashtekar and J. Lewandowski, "Background independent quantum gravity: A Status report," *Class. Quant. Grav.* **21** (2004) R53, [arXiv:gr-qc/0404018](https://arxiv.org/abs/gr-qc/0404018).
- [3] T. Thiemann, *Modern Canonical Quantum General Relativity*. Cambridge University Press, 2007.
- [4] C. Rovelli and F. Vidotto, *Covariant Loop Quantum Gravity: An Elementary Introduction to Quantum Gravity and Spinfoam Theory*. Cambridge University Press, 2014.

- [5] C. Rovelli, *Quantum gravity*. Cambridge university press, 2007.
- [6] M. Han, M. A. Yongge, and W. Huang, “FUNDAMENTAL STRUCTURE OF LOOP QUANTUM GRAVITY,” *International Journal of Modern Physics D* **16** (2005), no. 09, 1397–1474.
- [7] C. Rovelli and S. Speziale, “On the geometry of loop quantum gravity on a graph,” *Phys. Rev. D* **82** (2010) 044018, [arXiv:1005.2927](#).
- [8] L. Freidel and S. Speziale, “From twistors to twisted geometries,” *Phys. Rev. D* **82** (2010) 084041, [arXiv:1006.0199](#).
- [9] L. Freidel and S. Speziale, “Twisted geometries: A geometric parametrization of $SU(2)$ phase space,” *Phys. Rev. D* **82** (Oct, 2010) 084040.
- [10] G. Long and C.-Y. Lin, “Geometric parametrization of $SO(D+1)$ phase space of all dimensional loop quantum gravity,” *Phys. Rev. D* **103** (Apr, 2021) 086016.
- [11] G. Long, “Parametrization of holonomy-flux phase space in the Hamiltonian formulation of $SO(N)$ gauge field theory with $SO(D+1)$ loop quantum gravity as an exemplification,” [arXiv:2307.05542](#).
- [12] T. Regge, “General relativity without coordinates,” *Nuovo Cim.* **19** (1961) 558–571.
- [13] E. Alesci, M. Assanioussi, J. Lewandowski, and I. Mäkinen, “Hamiltonian operator for loop quantum gravity coupled to a scalar field,” *Phys. Rev. D* **91** (2015), no. 12, 124067, [arXiv:1504.02068](#).
- [14] M. Assanioussi, J. Lewandowski, and I. Mäkinen, “New scalar constraint operator for loop quantum gravity,” *Phys. Rev. D* **92** (2015), no. 4, 044042, [arXiv:1506.00299](#).
- [15] C. Zhang, S. Song, and M. Han, “First-Order Quantum Correction in Coherent State Expectation Value of Loop-Quantum-Gravity Hamiltonian,” *Phys. Rev. D* **105** (2022) 064008, [arXiv:2102.03591](#).
- [16] J. Yang and Y. Ma, “New Hamiltonian constraint operator for loop quantum gravity,” *Phys. Lett. B* **751** (2015) 343–347, [arXiv:1507.00986](#).
- [17] A. Perez, “The Spin Foam Approach to Quantum Gravity,” *Living Rev. Rel.* **16** (2013) 3, [arXiv:1205.2019](#).
- [18] M. Han, Z. Huang, H. Liu, and D. Qu, “Complex critical points and curved geometries in four-dimensional Lorentzian spinfoam quantum gravity,” *Phys. Rev. D* **106** (2022), no. 4, 044005, [arXiv:2110.10670](#).
- [19] M. Han and H. Liu, “Effective Dynamics from Coherent State Path Integral of Full Loop Quantum Gravity,” *Phys. Rev. D* **101** (2020), no. 4, 046003, [arXiv:1910.03763](#).
- [20] M. Han and H. Liu, “Semiclassical limit of new path integral formulation from reduced phase space loop quantum gravity,” *Phys. Rev. D* **102** (2020), no. 2, 024083, [arXiv:2005.00988](#).
- [21] G. Long and Y. Ma, “Effective dynamics of weak coupling loop quantum gravity,” *Phys. Rev. D* **105** (2022), no. 4, 044043, [arXiv:2111.11844](#).
- [22] A. Ashtekar and J. Lewandowski, “Quantum theory of geometry. 1: Area operators,” *Class. Quant. Grav.* **14** (1997) A55–A82, [arXiv:gr-qc/9602046](#).
- [23] A. Ashtekar and J. Lewandowski, “Quantum theory of geometry. 2. Volume operators,” *Adv. Theor. Math. Phys.* **1** (1998) 388–429, [arXiv:gr-qc/9711031](#).
- [24] Y. Ma, C. Soo, and J. Yang, “New length operator for loop quantum gravity,” *Phys. Rev. D* **81** (2010) 124026, [arXiv:1004.1063](#).
- [25] E. Bianchi, “The Length operator in Loop Quantum Gravity,” *Nucl. Phys. B* **807** (2009) 591–624, [arXiv:0806.4710](#).

- [26] G. Long and Y. Ma, “General geometric operators in all dimensional loop quantum gravity,” *Phys. Rev. D* **101** (2020), no. 8, 084032, [arXiv:2003.03952](#).
- [27] T. Thiemann, “Gauge field theory coherent states (GCS): I. General properties,” *Classical and Quantum Gravity* **18** (2001), no. 11,.
- [28] T. Thiemann and O. Winkler, “Gauge field theory coherent states (GCS): II. Peakedness properties,” *Classical and Quantum Gravity* **18** (2001), no. 14, 2561–2636.
- [29] E. Bianchi, E. Magliaro, and C. Perini, “Coherent spin-networks,” *Phys. Rev. D* **82** (2010) 024012, [arXiv:0912.4054](#).
- [30] A. Calcinari, L. Freidel, E. Livine, and S. Speziale, “Twisted geometries coherent states for loop quantum gravity,” *Classical and Quantum Gravity* **38** (Dec, 2020) 025004.
- [31] E. R. Livine and D. R. Terno, “Reconstructing quantum geometry from quantum information: Area renormalisation, coarse-graining and entanglement on spin networks,” [arXiv:gr-qc/0603008](#).
- [32] W. Donnelly, “Entanglement entropy in loop quantum gravity,” *Phys. Rev. D* **77** (2008) 104006, [arXiv:0802.0880](#).
- [33] W. Donnelly, “Decomposition of entanglement entropy in lattice gauge theory,” *Phys. Rev. D* **85** (2012) 085004, [arXiv:1109.0036](#).
- [34] W. Donnelly, “Entanglement entropy and nonabelian gauge symmetry,” *Class. Quant. Grav.* **31** (2014), no. 21, 214003, [arXiv:1406.7304](#).
- [35] E. Bianchi, L. Hackl, and N. Yokomizo, “Entanglement entropy of squeezed vacua on a lattice,” *Phys. Rev. D* **92** (2015), no. 8, 085045, [arXiv:1507.01567](#).
- [36] C. Delcamp, B. Dittrich, and A. Riello, “On entanglement entropy in non-Abelian lattice gauge theory and 3D quantum gravity,” *JHEP* **11** (2016) 102, [arXiv:1609.04806](#).
- [37] E. R. Livine, “Intertwiner Entanglement on Spin Networks,” *Phys. Rev. D* **97** (2018), no. 2, 026009, [arXiv:1709.08511](#).
- [38] B. Baytas, E. Bianchi, and N. Yokomizo, “Gluing polyhedra with entanglement in loop quantum gravity,” *Phys. Rev. D* **98** (2018), no. 2, 026001, [arXiv:1805.05856](#).
- [39] Q. Chen and E. R. Livine, “Intertwiner entanglement excitation and holonomy operator,” *Class. Quant. Grav.* **39** (2022), no. 21, 215013, [arXiv:2204.03093](#).
- [40] G. Long, C. Zhang, and X. Zhang, “Superposition type coherent states in all dimensional loop quantum gravity,” *Phys. Rev. D* **104** (Aug, 2021) 046014.
- [41] B. Hall, “The Segal-Bargmann "Coherent State" Transform for Compact Lie Groups,” *Journal of Functional Analysis* **122** (1994), no. 1, 103–151.
- [42] G. Long, X. Zhang, and C. Zhang, “Twisted geometry coherent states in all dimensional loop quantum gravity: I. Construction and Peakedness properties,” [arXiv:2110.01317](#).
- [43] G. Long, “Twisted geometry coherent states in all dimensional loop quantum gravity. II. Ehrenfest property,” *Phys. Rev. D* **106** (2022), no. 6, 066021, [arXiv:2204.03056](#).
- [44] E. R. Livine and S. Speziale, “A New spinfoam vertex for quantum gravity,” *Phys. Rev. D* **76** (2007) 084028, [arXiv:0705.0674](#).
- [45] G. Long, C.-Y. Lin, and Y. Ma, “Coherent intertwiner solution of simplicity constraint in all dimensional loop quantum gravity,” *Physical Review D* **100** (2019), no. 6, 064065.
- [46] A. M. Perelomov, *Generalized coherent states and their applications*. 1986.
- [47] G. Long and N. Bodendorfer, “Perelomov-type coherent states of $SO(D + 1)$ in all-dimensional loop quantum gravity,” *Phys. Rev. D* **102** (2020), no. 12, 126004, [arXiv:2006.13122](#).

- [48] E. Bianchi, P. Doná, and S. Speziale, “Polyhedra in loop quantum gravity,” *Phys. Rev. D* **83** (Feb, 2011) 044035.
- [49] G. Long and Y. Ma, “Polytopes in all dimensional loop quantum gravity,” *Eur. Phys. J. C* **82** (2022), no. 41,.
- [50] L. Freidel and E. R. Livine, “Spin networks for noncompact groups,” *J. Math. Phys.* **44** (2003) 1322–1356, [arXiv:hep-th/0205268](#).
- [51] C. Charles and E. R. Livine, “The Fock Space of Loopy Spin Networks for Quantum Gravity,” *Gen. Rel. Grav.* **48** (2016), no. 8, 113, [arXiv:1603.01117](#).
- [52] S. Deser, R. Jackiw, and G. ’t Hooft, “Three-Dimensional Einstein Gravity: Dynamics of Flat Space,” *Annals Phys.* **152** (1984) 220.
- [53] L. Freidel and E. R. Livine, “3D Quantum Gravity and Effective Noncommutative Quantum Field Theory,” *Phys. Rev. Lett.* **96** (2006) 221301, [arXiv:hep-th/0512113](#).
- [54] E. R. Livine and D. R. Terno, “The Entropic boundary law in BF theory,” *Nucl. Phys. B* **806** (2009) 715–734, [arXiv:0805.2536](#).
- [55] A. Ashtekar, J. Baez, A. Corichi, and K. Krasnov, “Quantum geometry and black hole entropy,” *Phys. Rev. Lett.* **80** (1998) 904–907, [arXiv:gr-qc/9710007](#).
- [56] A. Ashtekar, J. C. Baez, and K. Krasnov, “Quantum geometry of isolated horizons and black hole entropy,” *Adv. Theor. Math. Phys.* **4** (2000) 1–94, [arXiv:gr-qc/0005126](#).
- [57] J. Engle, A. Perez, and K. Noui, “Black hole entropy and SU(2) Chern-Simons theory,” *Phys. Rev. Lett.* **105** (2010) 031302, [arXiv:0905.3168](#).
- [58] S. Song, H. Li, Y. Ma, and C. Zhang, “Entropy of black holes with arbitrary shapes in loop quantum gravity,” *Sci. China Phys. Mech. Astron.* **64** (2021), no. 12, 120411, [arXiv:2002.08869](#).
- [59] A. Ghosh and A. Perez, “Black hole entropy and isolated horizons thermodynamics,” *Phys. Rev. Lett.* **107** (2011) 241301, [arXiv:1107.1320](#). [Erratum: *Phys.Rev.Lett.* 108, 169901 (2012)].
- [60] S. Song, G. Long, C. Zhang, and X. Zhang, “Thermodynamics of isolated horizons in loop quantum gravity,” *Phys. Rev. D* **106** (2022), no. 12, 126007, [arXiv:2205.09984](#).
- [61] A. Perez, “Statistical and entanglement entropy for black holes in quantum geometry,” *Phys. Rev. D* **90** (2014), no. 8, 084015, [arXiv:1405.7287](#). [Addendum: *Phys.Rev.D* 90, 089907 (2014)].